

**Investigation of Pile-Up and Delamination of Au Thin Films on Various Substrates and the Behavior of the Films Described by a Discontinuous Elastic Strain Model**

by

James Brandon Frye

A thesis submitted to the Graduate Faculty of  
Auburn University  
in partial fulfillment of the  
requirements for the Degree of  
Master of Science

Auburn, Alabama  
May 6, 2012

Keywords: nanoindentation, thin films, pile-up,  
delamination

Copyright 2012 by James Brandon Frye

Approved by

Barton Prorok, Committee Chair, Associate Professor of Material Engineering  
Dong-Joo Kim, Associate Professor of Material Engineering  
Ruel Overfelt, Professor of Material Engineering

## Abstract

A new method of accurately and reliably extracting the actual Young's modulus of a thin film on a substrate has been developed. The method is referred to as the discontinuous elastic interface transfer model. The method has been shown to work exceptionally well with films and substrates encompassing a wide range of elastic moduli and Poisson ratios. The advantage of the method is that it does not require a continuous stiffness method and can use the standard Oliver and Pharr analysis and the use of a predictive formula for determining the modulus of the film as long as the film thickness, substrate modulus and bulk Poisson ratio of the film are known. However, when there is much pile-up during the indentation process in a softer film, the experimental data does not follow the predictive formula but instead follows a similar model with a single Poisson ratio between the film and the substrate.

## Acknowledgments

I would like to thank Dr. Prorok for his support and guidance throughout this process. I would like to thank my committee members, Dr. Overfelt and Dr. Kim for their time and suggestions toward my thesis and research. I would also like to thank both the current and previous members of my group; Bo, Kevin, Nicole, Shakib, Madhu, MariAnne, Danny, Naveed and Dong. Thanks to all of the faculty and staff members past and present in Materials Engineering at Auburn University including Steve, Allison, Jenny and LC. I would also like to acknowledge and thank all of my friends in Auburn for their support. And lastly I would like to thank my family for all of the support and love they have shown me throughout my time here at Auburn University.

## Table of Contents

Abstract.....	ii
Acknowledgments .....	iii
List of Tables .....	vi
List of Illustrations.....	vi
List of Abbreviations .....	x
Chapter 1: Introduction.....	1
1.1 Overview .....	1
1.2 Thesis Structure.....	2
Chapter 2: Literature Review of Instrumented Thin Film Indentation.....	3
2.1 Instrumented Indentation Testing.....	3
2.2 Continuous Stiffness Measurement.....	7
2.3 Erroneous Contact Area .....	10
2.4 Modeling Thin Film Substrate Effects .....	12
Chapter 3: Material Selection .....	20
3.1 Material Selection and Their Mechanical Properties .....	20
Chapter 4: Experimental Setup and Fabrication.....	21
4.1 Film Deposition.....	21
4.2 Nanoindentation .....	26

Chapter 5: Results and Discussions .....	28
5.1 Experimental Nanoindentation Analysis.....	28
Chapter 6: Conclusions.....	50
References.....	52

## List of Tables

Table 2.1.1 Geometries of different indenter tips; C-f = centerline to face angle, d = indentation depth, and a = tip radius for cone and spherical indenters. <sup>[7]</sup> .....	4
Table 3.1.1 Material selections for film and substrates with desirable Young's modulus and Poisson's ratio .....	20
Table 4.2.1 Sputtering parameters of 480 nm Au film with Ti adhesion layer .....	24

## List of Illustrations

Figure 2.1.1 Schematic of nanoindentation system. ....	3
Figure 2.1.2 Micrograph of a Berkovich indenter tip .....	5
Figure 2.1.3 (a) Load versus displacement plots for a typical, a relatively soft, and a relatively hard material. (b) Cross-sectional schematic of certain stages of the loading-unloading curve as shown in the typical load versus displacement plot. <sup>[7]</sup> .....	6
Figure 2.2.1 Load-Displacement curve during the continuous stiffness method. <sup>[8]</sup> .....	7
Figure 2.2.2a Young's Modulus versus Displacement into surface for a bulk material <sup>[9]</sup> .....	8
Figure 2.2.2b Young's Modulus versus Displacement into surface for a compliant film on hard substrate <sup>[9]</sup> .....	9
Figure 2.2.2c Young's Modulus versus Displacement into surface for a hard film on compliant substrate. <sup>[9]</sup> .....	10
Figure 2.3.1 Schematics of the pile-up and sink-in effect. ....	11
Figure 2.4.1 Schematic of a indentation's cross section showing $h$ , $h_f$ , $h_c$ , and $h_s$ and how they relate to indentation depth and elastic recovery after removal of load $P$ . <sup>[11]</sup> .....	14
Figure 2.4.2 (a) Schematic illustrating the concept of continuous transfer of strain between the film and substrate, (b) simulation indicating that strain discontinuously transferred between the film and substrate, and (c) schematic showing how the film and substrate components are decoupled in the discontinuous elastic interface transfer model. <sup>[7]</sup> .....	15
Figure 2.4.3 Finite element analysis of the $AlO_x$ film/substrate composites showing the elastic strain distribution for an indent penetrating 5nm into each film; (a) $SiO_2$ , (b), Ge, (c) Si, (d) MgO, and (e) Sapphire.....	17
Figure 2.4.4 $E-h$ curves of $AlO_x$ films on $SiO_2$ , Ge, Si, MgO and $Al_2O_3$ showing a flat region at low indentation depths .....	18
Figure 2.4.5 Zhou et al. demonstrating that the film's modulus does not correspond to $E_{flat}$ that their second model has the ability to accurately extract film modulus from the composite nanoindentation data. ....	19

Figure 4.1.1 Schematic of sputtering method .....	22
Figure 4.1.2 Denton Vacuum Inc. DC & RF sputtering system. ....	23
Figure 4.1.3 Tencor Instruments "Alpha-Step 200" profilometer. ....	25
Figure 4.2.1 Image of MTS Nano Indenter XP nanoindentation system.....	27
Figure 5.1.1 <i>E-h</i> curve of arbitrary film on substrate with varying film Modulus .....	29
Figure 5.1.2 <i>E-h</i> curve of arbitrary film on substrate with varying substrate modulus .....	30
Figure 5.1.3 <i>E-h</i> curve of arbitrary film on substrate with varying film Poisson ratio.....	32
Figure 5.1.4 <i>E-h</i> curve of arbitrary film on substrate with varying substrate Poisson ratio .....	33
Figure 5.1.5 <i>E-h</i> curve of arbitrary film on substrate showing combined effect of varying Poisson ratios of film and substrate.....	34
Figure 5.1.6a <i>E-h</i> curve for Al <sub>2</sub> O <sub>3</sub> substrate. ....	36
Figure 5.1.6b <i>E-h</i> curve for MgO substrate. ....	36
Figure 5.1.6c <i>E-h</i> curve for Si substrate. ....	37
Figure 5.1.6d <i>E-h</i> curve for SiO <sub>2</sub> substrate. ....	37
Figure 5.1.6e <i>E-h</i> curve for Ge substrate. ....	38
Figure 5.1.7 <i>E-h</i> curve for Au on 5 different substrates. ....	39
Figure 5.1.8 <i>E-h</i> curve with discontinuous model and film E for 500nm Au on Ge with Ti adhesion layer. ....	40
Figure 5.1.9 $\alpha$ - <i>h</i> curve for 500nm Au on Ge with Ti adhesion layer.....	40
Figure 5.1.10 <i>E-h</i> curve with discontinuous model and film E for 500nm Au on Si with Ti adhesion layer. ....	41
Figure 5.1.11 $\alpha$ - <i>h</i> curve for 500nm Au on Si with Ti adhesion layer.....	41
Figure 5.1.12 <i>E-h</i> curve with discontinuous model and film E for 500nm Au on MgO with Ti adhesion layer. ....	42
Figure 5.1.13 $\alpha$ - <i>h</i> curve for 500nm Au on MgO with Ti adhesion layer.....	42
Figure 5.1.14 <i>E-h</i> curve with discontinuous model and film E for 500nm Au on Al <sub>2</sub> O <sub>3</sub> with Ti adhesion layer. ....	43



Figure 5.1.13 $\alpha$ -h curve for 500nm Au on Al <sub>2</sub> O <sub>3</sub> with Ti adhesion layer.....	43
Figure 5.1.15 E-h curve with Z-P model, film E, and film alpha for 2000nm Au on SiO <sub>2</sub> .....	44
Figure 5.1.16 E-h curve with discontinuous model and D-N model for 2000nm Au on SiO <sub>2</sub> . ...	45
Figure 5.1.17 JEOL JSM 7000F Scanning Electron Microscope.....	46
Figure 5.1.18 Micrograph of 2000nm Au on SiO <sub>2</sub> 370nm indentation.....	47
Figure 5.1.19 Micrograph of 2000nm Au on SiO <sub>2</sub> 500nm indentation.....	47
Figure 5.1.20 Micrograph of 2000nm Au on SiO <sub>2</sub> 800nm indentation.....	48
Figure 5.1.21 Micrograph of 2000nm Au on SiO <sub>2</sub> 1000nm indentation.....	48
Figure 5.1.22 Micrograph of 2000nm Au on SiO <sub>2</sub> 1500nm indentation.....	49
Figure 5.1.23 Micrograph of 2000nm Au on SiO <sub>2</sub> 1700nm indentation.....	49

## List of Abbreviations

$E$	Composite Young's Modulus
DC	Direct Current
RF	Radio Frequency
D-N	In relation to Doerner and Nix Model
O-P	In relation to Oliver and Pharr Model
Z-P	In relation to Zhou and Prorok Model
S-N	In relation to Saha and Nix Model
$f$	As subscript: of the film
$i$	As subscript: of the indenter
Å	Angstrom
nm	Nanometer
$\varphi$	Weighting factor
$s$	As subscript: of the substrate
$\mu$	Shear Modulus
$\nu$	Poisson's Ratio
SEM	Scanning Electron Microscope
CSM	Continuous Stiffness Method
MEMS	Microelectromechanical systems

## Chapter 1: Introduction

### 1.1 Overview

Over the past several decades, Instrumented Indentation Testing (IIT) has become a heavily researched topic in both bulk and nano-scale material testing. From indentation tests, researchers can measure physical properties of materials such as the hardness and young's modulus. The areas of micro and nano-scale indentation has certainly gained more attention and focus in a world becoming more and more dependent and fascinated with smaller scale devices such as nanoparticles, nanowires, MEMS and NEMS devices. The computer and technology boom of the past several decades have led scientists and researchers to explore the properties and behavior of thin films. However, there are still several areas in thin film indentation that present problems in current measurement techniques. One of the main issues being investigated in micro and nano scale thin film indentation is the effect the substrate has on the measurements of the film. As a thin film becomes increasingly thin, the substrate's interaction with the properties and measurements of the film increases.

In the following work, the workings of Doerner, Nix, Gao, Oliver and Pharr were studied in order to build off of their findings and understand the behavior of thin films more clearly. The complexity of thin film Nanoindentation experimental and theoretical methods arise from many different phenomena including pile-up and sink-in of the film during Nanoindentation as well as microstructural effects such as grain size and orientation of thin films. In order to eliminate such microstructural problems in the experiments, a nanocrystalline film was used in the research to understand the substrate effect on the film and the resulting composite modulus. Five different substrates were chosen for the experiment with a range of Poisson ratios and Young's moduli.

## 1.2 Thesis Structure

Chapter 2 includes a literature review of all of the work related to this Thesis. It includes; instrumented indentation testing, continuous stiffness measurement, erroneous contact area, pile-up/sink-in effects during nanoindentation and major models that have been developed to extract the film's intrinsic properties. Chapter 3 discusses the selection of materials used in the research and why they were chosen. Chapter 4 details the experimental setup of the research including; how the samples were prepared, thin film deposition via sputtering techniques as well as the parameters used in the deposition process and overview of the Nanoindentation set-up. Chapter 5 presents the results of the experiments and discusses the meaning of the results and Chapter 6 gives a summary of the research.

## Chapter 2: Literature Review of Instrumented Thin Film Indentation

### 2.1 Instrumented Indentation Testing

Nanoindentation, or Instrumented Indentation Testing (IIT), is a high-resolution process of mechanically measuring a material's properties by driving an indenter tip made of diamond into the surface of a sample. During Nanoindentation, the indenter tip penetrates the sample as the load and displacement of the tip are recorded by positional sensors. From the measured recordings, the mechanical properties of the sample can be extracted. A schematic of a general Nanoindentation set-up is shown in Figure 2.1.1. The load from the tip is generated by a magnet and coil, and the displacement of the indenter is measured by a capacitive displacement gauge<sup>[8]</sup>.

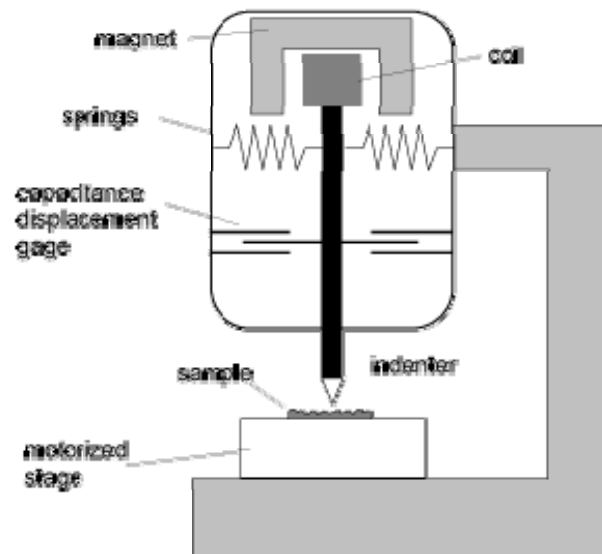







Figure 2.1.1 Schematic of nanoindentation system.<sup>[8]</sup>

There are several different types of indenter tips commonly used in Nanoindentation. However, the most common tip used is a Berkovich tip, or three sided pyramid. The advantage

of this tip is that it can be easily fabricated to a very sharp point by simple grinding techniques. In the case of the Vickers tip, or four sided pyramid, it is extremely hard to fabricate a sharp point and instead results in a wedge shape tip, which is used in some indentation experiments. Also, the Berkovich tip is geometrically self-similar, meaning that the geometry of the tip's cross section, normal to the sample being indented, remains unchanged as the tip penetrates further into the sample. Table 2.1.1 shows schematics of various tips used in indentation as well as their projected contact areas as a function of indent depth. [7]

Table 2.1.1 Geometries of different indenter tips; C-f = centerline to face angle, d = indentation depth, and a = tip radius for cone and spherical indenters. [7]

Parameter	Berkovich	Cube-corner	Cone	Spherical	Vickers
Shape					
C-f angle	65.35°	35.264°	—	—	68°
Projected Contact area	$24.5600d^2$	$2.5981d^2$	$\pi a^2$	$\pi a^2$	$24.5044d^2$

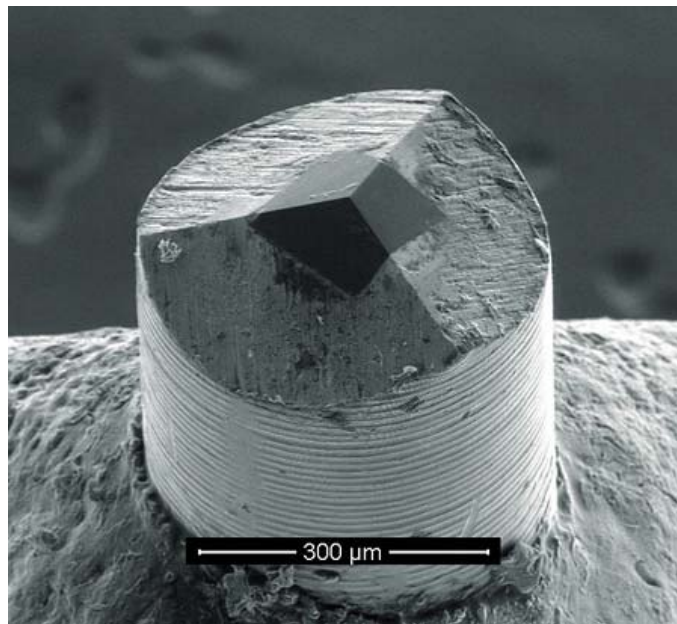


Figure 2.1.2 Micrograph of a Berkovich indenter tip

As the indenter penetrates the sample, there are two things happening congruently, plastic deformation and elastic deformation. As the tip is extracted from the sample, there is only the elastic response resulting in a force on the tip from the elastic recovery of the material being indented. This elastic recovery is related to how stiff the material is and the magnitude of the force on the tip is proportional to the elastic recovery. As the tip retracts from the sample, the elastic deformation is isolated from the total deformation and thus a curve of load versus displacement is used to determine the stiffness of the material. Equation 1 shows the relationship between the Stiffness,  $S$ , and the Reduced Young's modulus,  $E_r$ , with  $A$  being the projected contact area of the indenter tip.

$$S = \frac{dP}{dh} = \frac{2}{\sqrt{\pi}} E_r \sqrt{A} \quad (1)$$

From the equation, it can be seen that the stiffness of the material can be obtained by taking the instantaneous slope at the point of unloading, which is  $dP$ , or change in load, over  $dh$ , the change in indent depth. Using the model developed by Doerner and Nix, the modulus of the film can be extracted by relating the effective Young's modulus to the following equation:

$$\frac{1}{E_r} = \frac{(1 - \nu^2)}{E} + \frac{(1 - \nu_i^2)}{E_i} \quad (2)$$

where  $E$  is the modulus of the film,  $E_i$  is the modulus of the indenter tip,  $\nu$  is the Poisson ratio of the film and  $\nu_i$  is the Poisson ratio of the indenter tip. Figure 2.1.3 represents load versus

displacement plots for a material that is relatively soft as well as a plot of a material that is relatively hard, or stiff. [7]

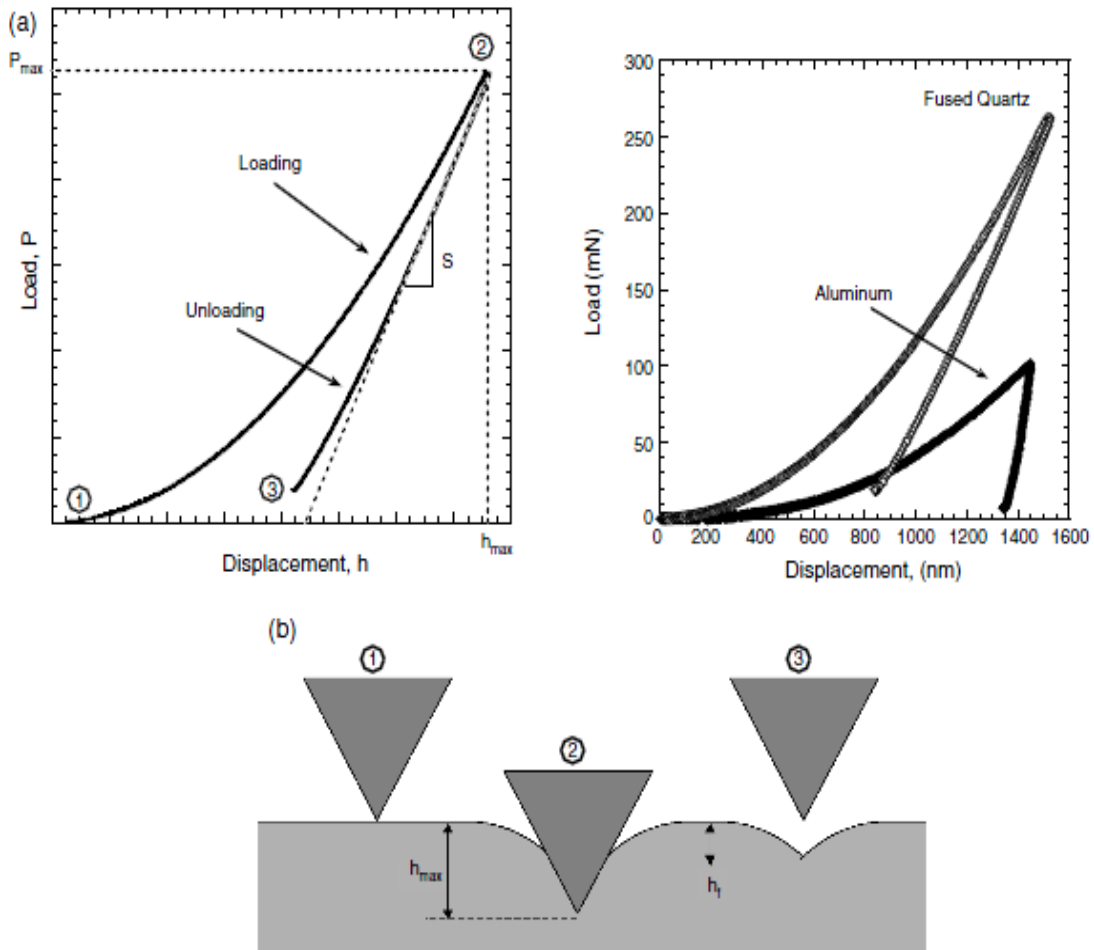


Figure 2.1.3 (a) Load versus displacement plots for a typical, a relatively soft, and a relatively hard material. (b) Cross-sectional schematic of certain stages of the loading-unloading curve as shown in the typical load versus displacement plot. [7]



## 2.2 Continuous Stiffness Measurement

The Continuous Stiffness Measurement, or CSM, is an indentation method where the indenter oscillates up and down onto the sample with an increasing load. This method is useful in Nanoindentation of thin films in that the method can accurately extract the modulus of the sample at a finite number of indentation depths. The result of the continuous stiffness measurement is that the test gives a curve of the modulus at each depth as the indenter pulls away from the sample and measures the force from the samples elastic spring back, or elastic recovery. CSM allows for the separation of the film and the substrates corresponding properties such as hardness and modulus. Figure 2.2.1 shows a load versus displacement curve of a theoretical indentation test, where each spike in the curve represents a single oscillation and measurement of stiffness.

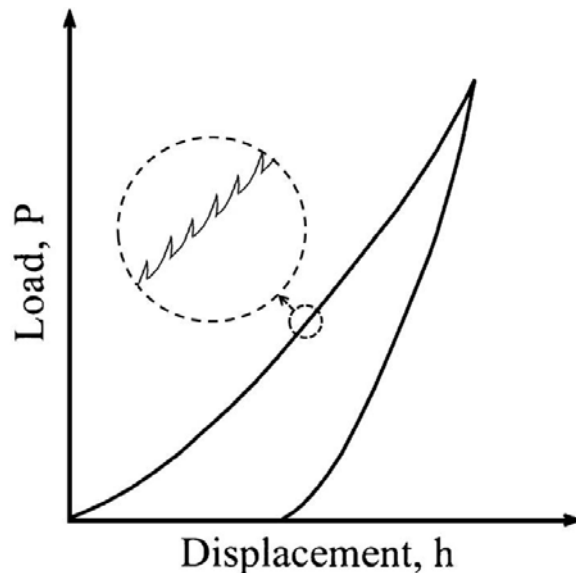


Figure 2.2.1 Load-Displacement curve during the continuous stiffness method.<sup>[8]</sup>

In the case of the CSM method, instead of getting a single value for the modulus, it is possible to get a progressive measurement at each individual indent depth. The result of the plot, for a thin film on a substrate, shows that at lower depths, the value of the recorded modulus is

more characteristic of the film while at higher indent depths, the recorded modulus is characteristic of the substrate. At intermediate depths, the modulus is a mixture of the film and the substrate moduli as the two components interact with each other. When indenting that of a bulk material, the resulting plot will exhibit a horizontal line representing the value of the modulus. As for a compliant film on a hard substrate, the corresponding plot will exhibit an increase in modulus as the indenter's depth increases. Conversely, in the case of a hard film on a soft substrate, the plot will exhibit a decreasing trend as the elastic recovery against the indenter decreases the closer it gets to the substrate. Figure 2.2.2a-c represents CSM indentation plots of a bulk material, soft film on a hard substrate and a hard film on a soft substrate respectively.

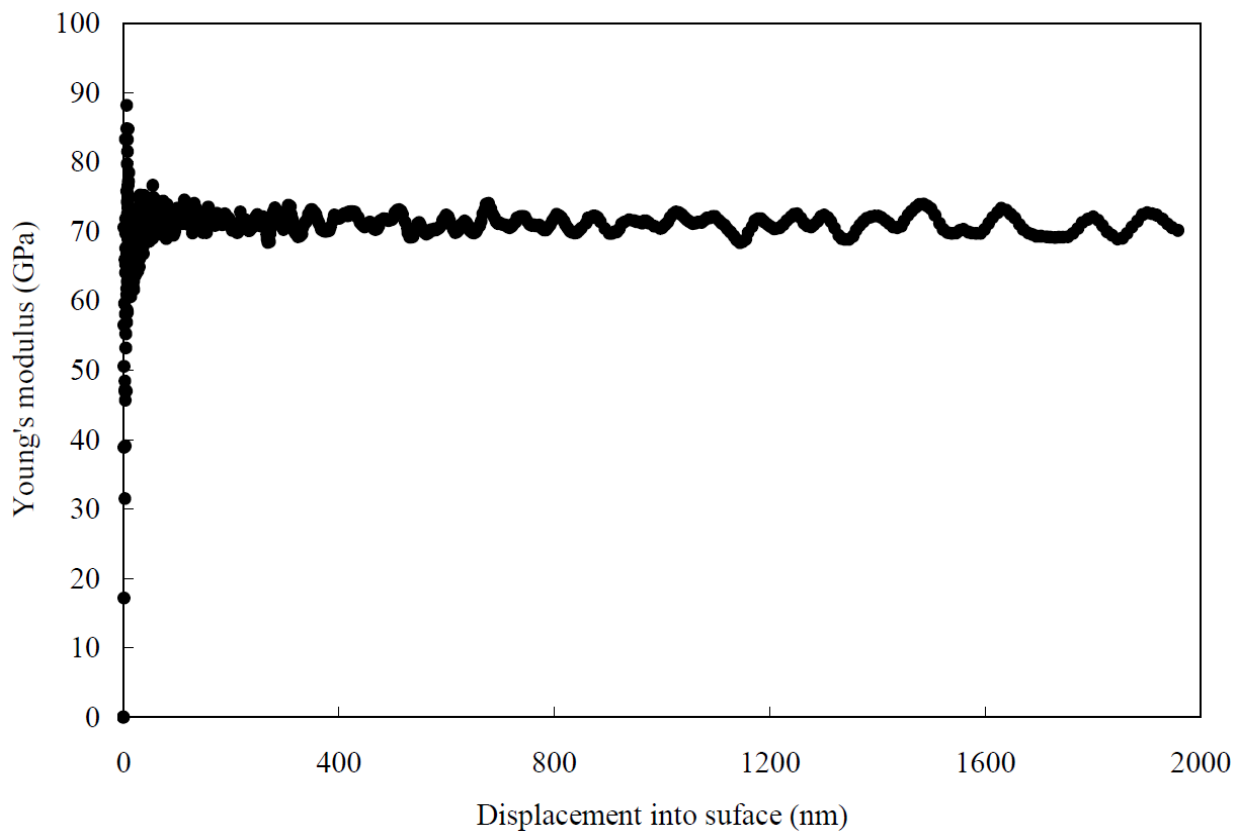


Figure 2.2.2a Young's Modulus versus Displacement into surface for a bulk material <sup>[9]</sup>

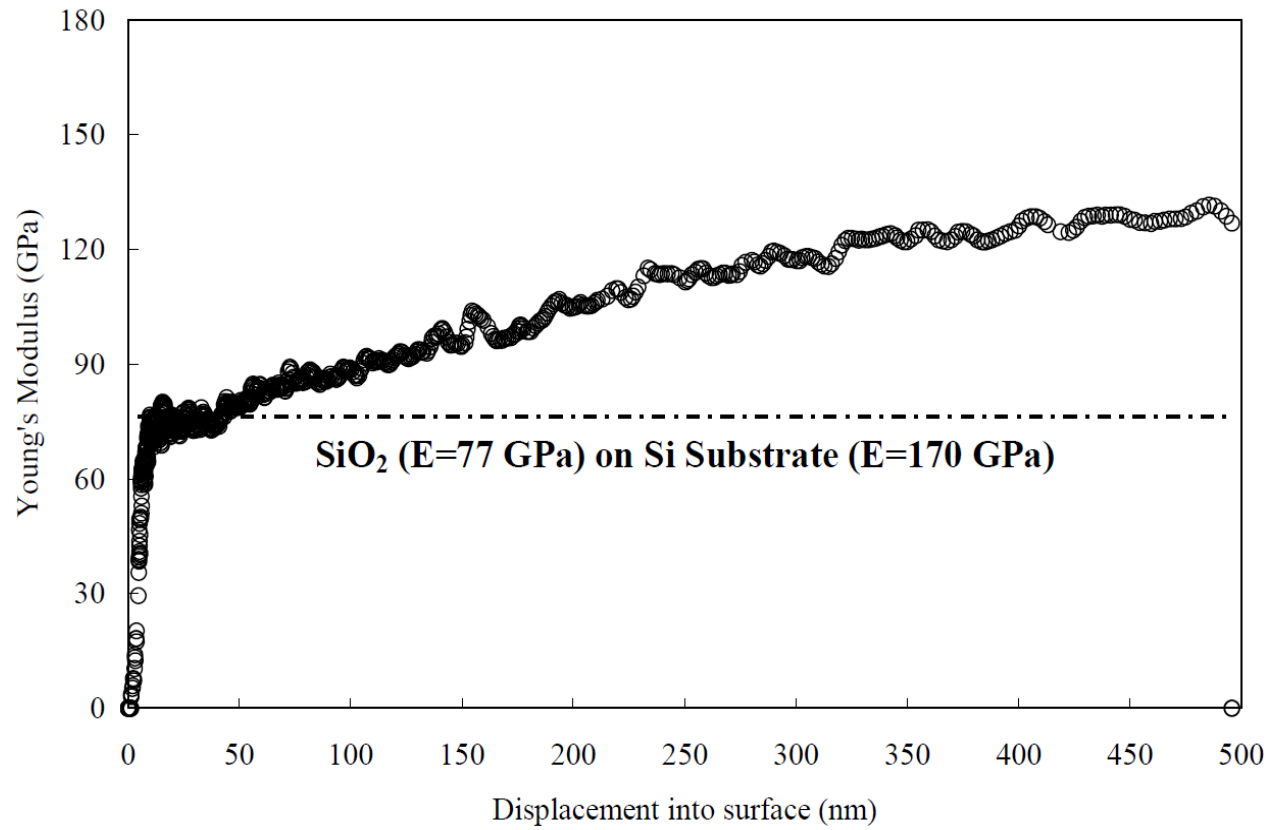


Figure 2.2.2b Young's Modulus versus Displacement into surface for a compliant film on hard substrate<sup>[9]</sup>

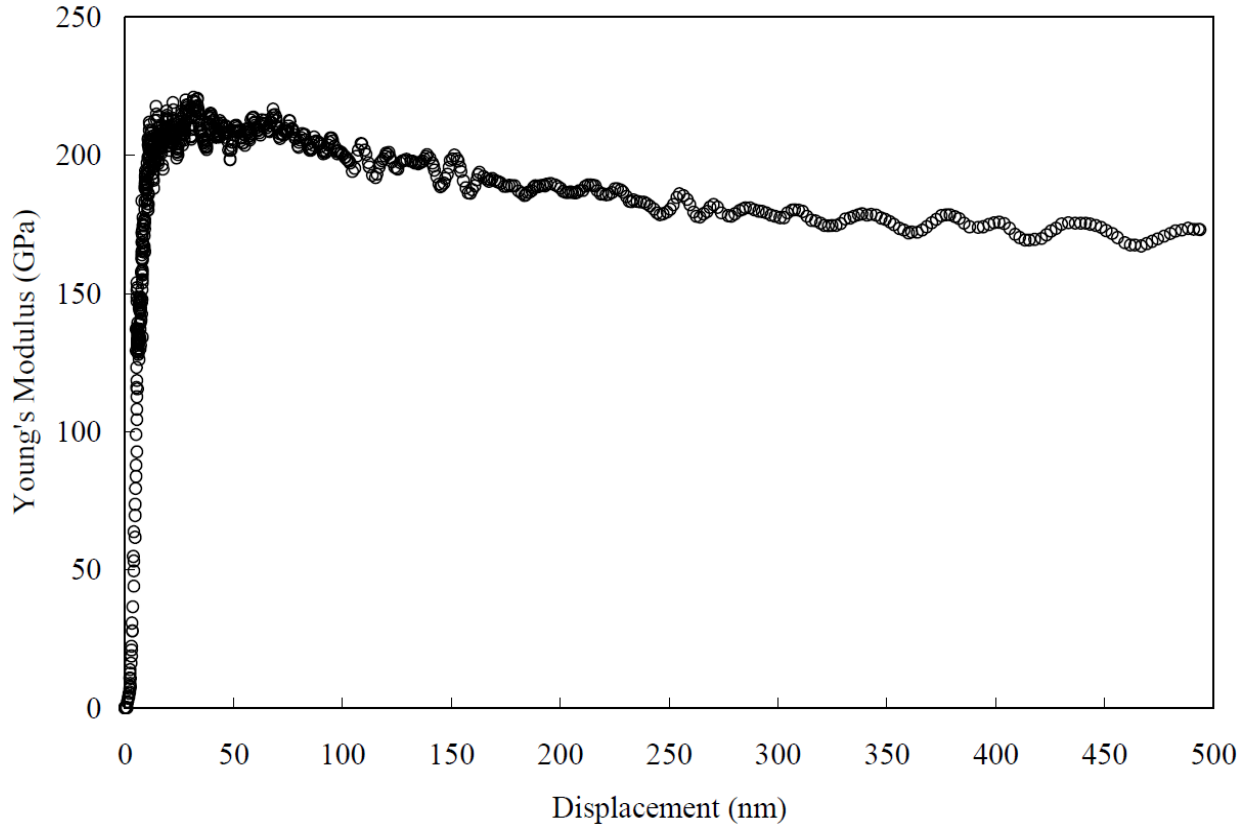


Figure 2.2.2c Young's Modulus versus Displacement into surface for a hard film on compliant substrate. <sup>[9]</sup>

### 2.3 Erroneous Contact Area

There exists a great problem in Nanoindentation tests due to a physical concept known as erroneous contact area. Since the measured modulus and hardness values of a sample are dependent on the projected contact area of the indenter's tip, any deviation away from an increase in contact area as described by a known function of indentation depth will result in a misrepresentation of the measured stiffness. In the case of a soft film on a relatively hard substrate, the film material has a tendency to "pile-up" around the edges of the indenter tip, resulting in an underestimation of the projected contact area and an overestimation of the calculated modulus and hardness. The reason for the overestimation, in this case, is due to more

material providing elastic recovery than what the projected contact area would suggest. On the other hand, in the case of a hard material on a relatively soft substrate, there exists a “sink-in” effect. The sink-in effect arises from the harder film material projecting its strain into the substrate causing an underestimation in the projected contact area from what the function of the indent depth would suggest. An underestimation of the projected contact area leads to an underestimation in the modulus and hardness due to less material contributing to the elastic recovery at a given indent depth. Figure 2.3.1 depicts a schematic of both a pile-up effect and sink-in effect as well as what the corresponding cross-sectional area,  $A_i$ , of the indenter looks like. <sup>[10]</sup>

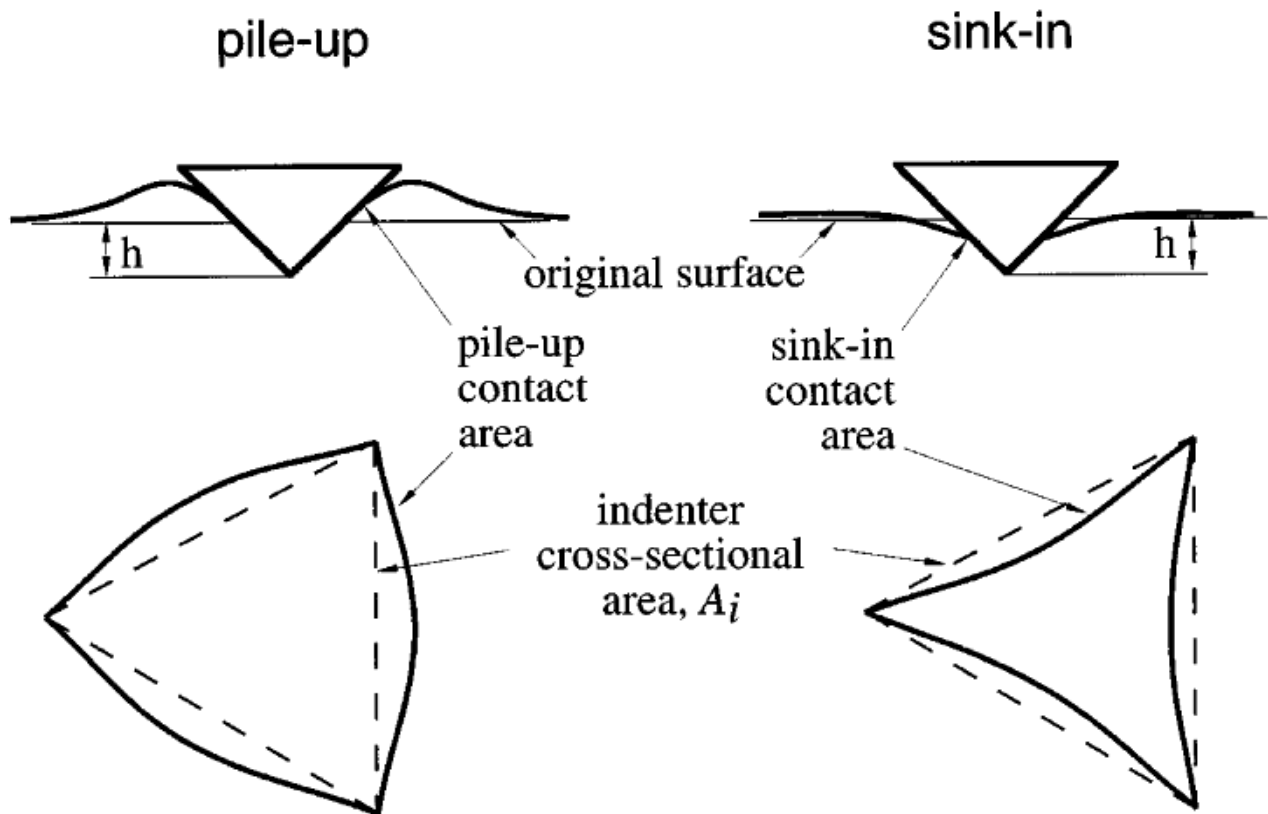


Figure 2.3.1 Schematics of the pile-up and sink-in effect. <sup>[10]</sup>

## 2.4 Modeling Thin Film Substrate Effects

Instrumented indentation testing has become increasingly difficult to characterize and model as the science has become more focused on the nanoscale regime. The problem arises from the influence that the substrate has on the thin film at the nanoscale. Because of the interactions between the thin film and substrate, it becomes a difficult task to isolate and extract the film's properties at such shallow indentation depths. Many researchers have formulated theories and models in order to deal with the underlying problem of the thin film/substrate interaction.<sup>[1, 2, 5, 7, 11, 12]</sup> Some of the models do a good job of explaining certain combinations of films and substrates, however, there hasn't been a specific model that can describe the behavior of most thin film/substrate combinations accurately.

Oliver and Pharr found there to be a power law function describing the stiffness curve which states for most materials, the unloading load-displacement curve is not linear:

$$P = B(h - h_f)^m \quad (3)$$

where  $P$  is the load,  $B$  and  $m$  are empirically determined constants and  $h_f$  is the final displacement after the elastic recovery of the material.<sup>[11]</sup>

With the stiffness measurements and projected contact area, at a certain indentation depth, the reduced modulus and hardness can be calculated using the following relationship:

$$E_r = \frac{\sqrt{\pi}}{2} \frac{S}{\sqrt{A}} \quad (4)$$

And

$$H = \frac{P}{A} \quad (5)$$

Where  $S$  is the stiffness,  $E_r$  is the reduced modulus and  $A$  is the projected contact area at a peak load and a function of  $h_c$ , or the indentation depth:

$$A = 24.5h_c^2 \quad (6)$$

The area function in the form of  $A = f(h_c)$ , assumes a perfect Berkovich indenter tip. However, there cannot be such a perfect tip and so the following equation more accurately describes the projected contact area as a function of indent depth:

$$A = 24.5h_c^2 + C_1h_c^1 + C_2h_c^{1/2} + C_3h_c^{1/4} + \dots + C_8h_c^{1/128} \quad (7)$$

Where  $C_1 - C_8$  are constants, with the leading term describing that of an unblunted Berkovich indenter.

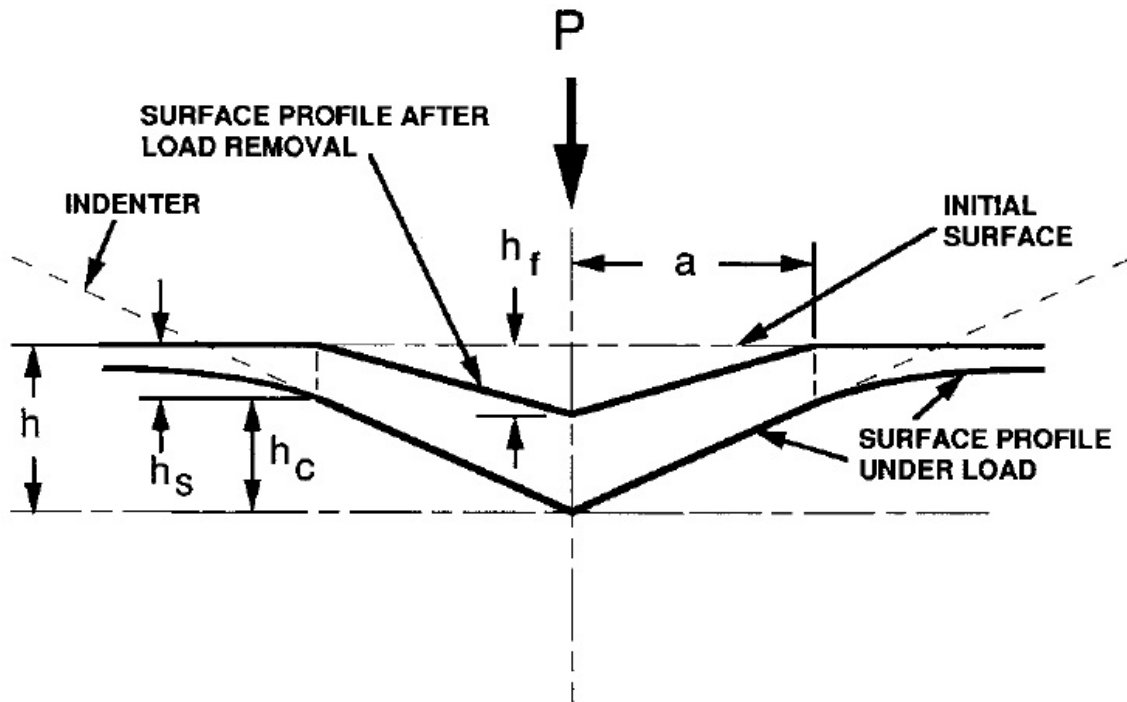


Figure 2.4.1 Schematic of a indentation's cross section showing  $h$ ,  $h_f$ ,  $h_c$ , and  $h_s$  and how they relate to indentation depth and elastic recovery after removal of load  $P$ .<sup>[11]</sup>

Doerner and Nix developed a model to extract the film modulus from the composite modulus.<sup>[1]</sup> In their model, they suggested that there is a continuous transfer of energy between the film and the substrate at the interface. A continuous transfer of energy suggests that the strain at the interface on the film side is equal to the strain at the substrate side. Figure 2.4.2a shows a schematic of a completely continuous transfer of energy from the film to the substrate and equal magnitudes of strain at the interface. Due to a continuous transfer of energy, their model uses a single weighting factor,

$$\frac{1}{E'} = \frac{1}{E'_f} + \left( \frac{1}{E'_s} - \frac{1}{E'_f} \right) \varphi_{D-N} \quad (8)$$

Where  $E'$  is the composite modulus,  $E'_f = E_f / (1 - \nu_f^2)$  is the film modulus,  $E'_s = E_s / (1 - \nu_s^2)$  is the substrate modulus and  $\varphi_{D-N}$  is the Doerner and Nix weighting factor. The weighting factor describes that the substrates effect on the composite modulus increases as the indenter penetrates further into the film, approaching the substrate,

$$\varphi_{D-N} = e^{-\alpha(t/h_{eff})} \quad (9)$$

Where  $\alpha$  is suggested to be an empirically determined constant,  $t$  is the film's thickness and  $h_{eff}$  is the effective indentation depth, or depth at which the projected contact area represents.

Doerner and Nix suggested that for most materials,  $\alpha$  can be assumed to be equal to around 0.25.



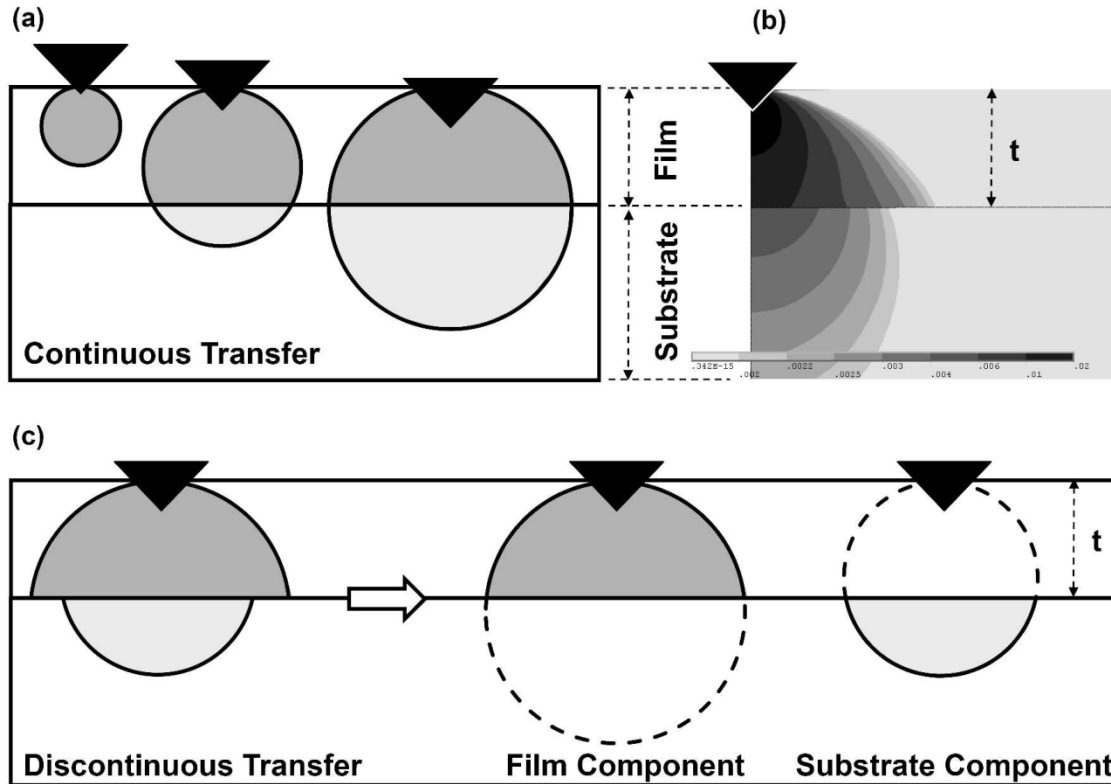


Figure 2.4.2 (a) Schematic illustrating the concept of continuous transfer of strain between the film and substrate, (b) simulation indicating that strain discontinuously transferred between the film and substrate, and (c) schematic showing how the film and substrate components are decoupled in the discontinuous elastic interface transfer model.<sup>[7]</sup>

However, Zhou and Prorok found that there is not a continuous transfer of energy between the film and the substrate. Finite element analysis was used to show that the transfer of energy at the interface is discontinuous. Figure 2.4.3 show simulations of AlOx films on various substrates, and how the strain fields change across the film substrate interface. As described by the discontinuous model, there has to be two weighting factors accounted for in the composite

modulus. Building from the models of Doerner and Nix and Gao, the discontinuous model has the following form,

$$\frac{1}{E'} = \frac{1}{E'_f} (1 - \varphi_s) + \frac{1}{E'_s} \varphi_f \quad (10)$$

where,

$$\varphi_f = e^{-\alpha_f(t/h)} \text{ and } \varphi_s = e^{-\alpha_s(t/h)} \quad (11)$$

Here  $\varphi_f$  and  $\varphi_s$  represent the weighting factors of the film and substrate respectively, which account for the effects of the film on the substrate as well as the substrate on the film. The weighting factors' physical meanings are represented in figure 2.4.2c. The terms  $\alpha_f$  and  $\alpha_s$  are the film and substrate constants, which are equal to the Poisson's ratios of the film and substrate respectively.

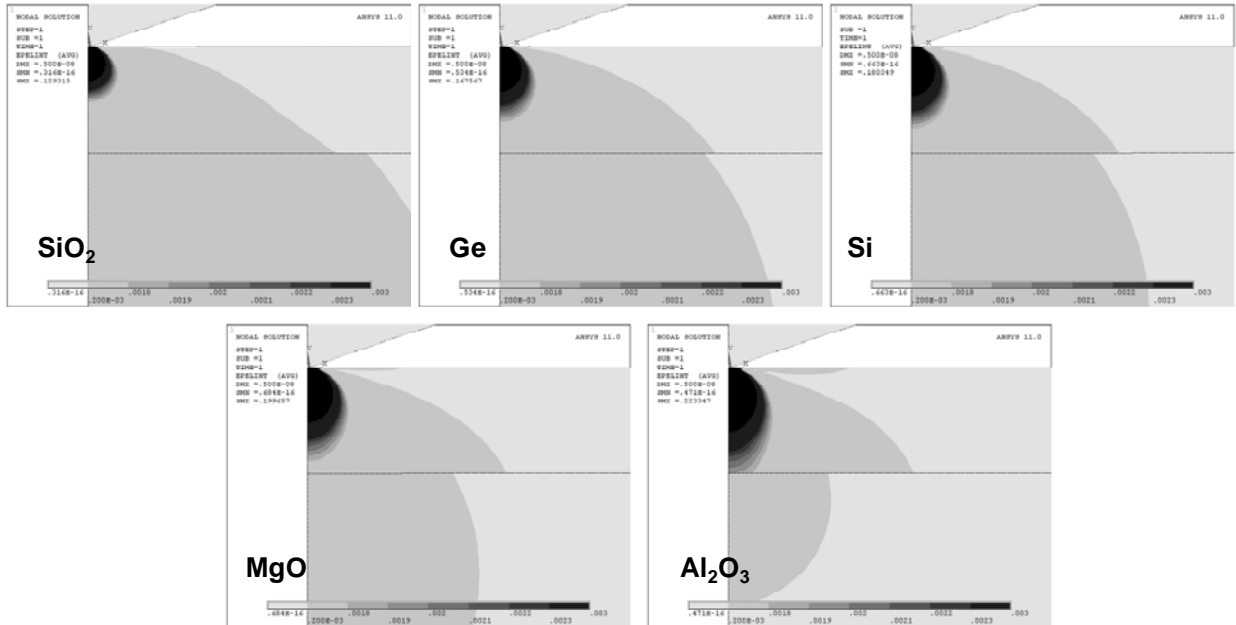


Figure 2.4.3 Finite element analysis of the AlO<sub>x</sub> film/substrate composites showing the elastic strain distribution for an indent penetrating 5nm into each film; (a) SiO<sub>2</sub>, (b), Ge, (c) Si, (d) MgO, and (e) Sapphire

However, Zhou et. al. found that there was a flat region at very shallow indentation depths where the initial value of the modulus at low indentation depths is believed to be representative of the Young's modulus of the film. Further investigation shows that upon increasing indentation depth, the value of the composite modulus increases or decreases as the effect of the substrate increases with depth. In the flat region, or  $E'_{flat}$ , the modulus is highly dependent on the substrate modulus, increasing with increasing substrate moduli. Figure 2.4.3 shows  $E-h$  curves of AlO<sub>x</sub> films on SiO<sub>2</sub>, Ge, Si, MgO and Al<sub>2</sub>O<sub>3</sub> showing a flat region at low indentation depths. [7]

$$\frac{1}{E'} = \frac{1}{E'_f} (1 - \varphi_s) \left( \frac{E'_f}{E'_s} \right)^{0.1} + \frac{1}{E'_s} \varphi_f \quad (12)$$

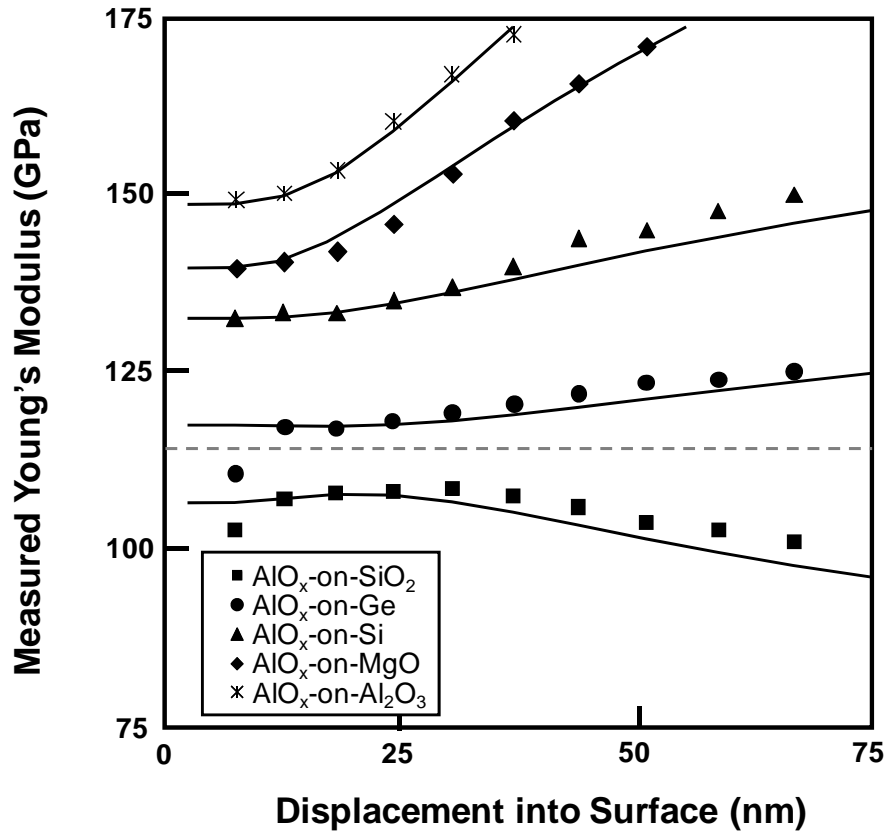


Figure 2.4.4 *E-h* curves of AlO<sub>x</sub> films on SiO<sub>2</sub>, Ge, Si, MgO and Al<sub>2</sub>O<sub>3</sub> showing a flat region at low indentation depths

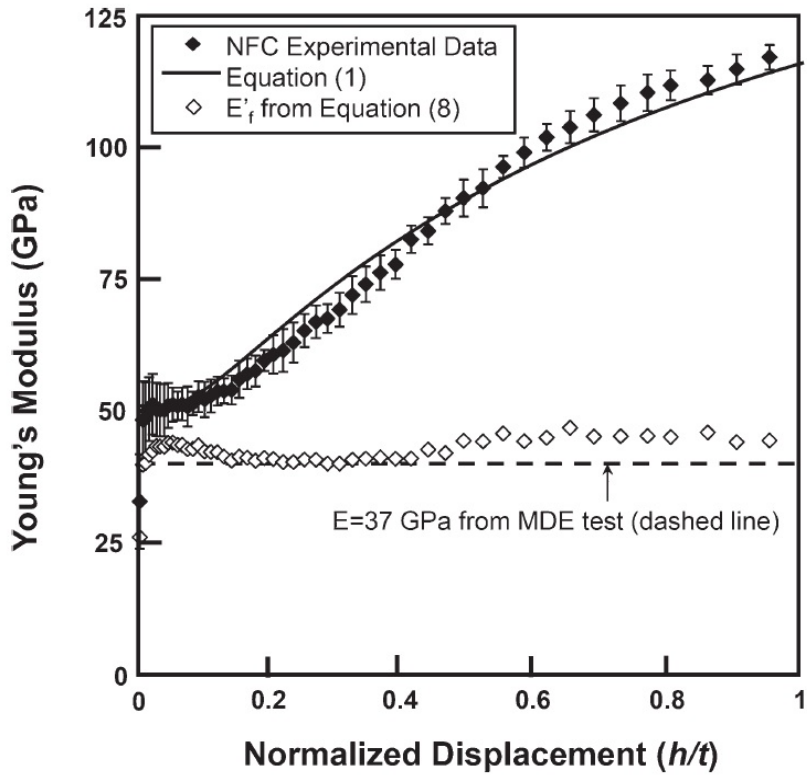


Figure 2.4.5 Zhou et al. demonstrating that the film's modulus does not correspond to  $E_{flat}$  that their second model has the ability to accurately extract film modulus from the composite nanoindentation data.

## Chapter 3: Material Selection

### 3.1 Material Selection and Their Mechanical Properties

The substrates that were investigated in this work were chosen based upon a couple of different parameters. A list of the selected substrates is shown in Table 3.1.1. In order to explore how the composite modulus of a film on a substrate behaves, the substrate candidates needed to have a range of properties differing from that of the Au film. Since the discontinuous model was being investigated, the chosen substrates had Young's moduli ranging from near the value of gold's modulus to several times that. The Poisson's ratios of the chosen substrates were all chosen to be less than or equal to that of gold. MgO was chosen due to it having a bulk Poisson ratio equal to the value of Au, but has a higher Young's modulus. Si was chosen based off of it having a higher Poisson ratio as well as a higher Young's modulus relative to Au as well as the fact that the properties of Si are widely known and would serve as a benchmark for other tests. Al<sub>2</sub>O<sub>3</sub> had a Poisson ratio close to that of Si but a much higher Young's modulus. And finally, SiO<sub>2</sub> was investigated due to having a similar Young's modulus relative to Au, but a much lower Poisson's ratio. The Au/SiO<sub>2</sub> combination would become the main focus of this work, as its Nanoindentation data would result in a very unique trend compared to the rest of the data.

Table 3.1.1 Material selections for film and substrates with desirable Young's modulus and Poisson's ratio

Film			Substrates		
Material	E (GPa)	$\nu$	Material	E (GPa)	$\nu$
Au	78	0.44	MgO	270-330	0.18
			Si	165	0.27
			Al <sub>2</sub> O <sub>3</sub>	430-460	0.21-0.27
			Ge	135	0.26
			SiO <sub>2</sub>	78	0.18

## Chapter 4: Experimental Setup and Fabrication

### 4.1 Film Deposition

There are many ways to deposit or grow materials on substrates such as sputtering, e-beam lithography, plasma enhanced chemical vapor deposition (PECVD), low pressure chemical vapor deposition (LPCVD) and so on. In this work, magnetron sputtering was chosen for the film deposition method. Magnetron sputtering is a physical deposition process in which ion bombardment is the primary mechanism for the film growth. In this method, argon gas is introduced into the chamber and either an RF or DC power supply is used to create an argon plasma. The argon plasma sputters a graphite electrode, where the target material is located, and a magnetic field is applied in order to increase the mean free path of the electrons by spiraling the electrons. The increase in mean free path increases the deposition rate of the target material. A voltage bias can be applied to the substrate to increase the ion bombardment, and hence increase the deposition rate. When sputtering, there are several parameters than can affect the quality of the deposited film such as chamber pressure, RF or DC wattage and argon flow rate, to name a few, which make sputtering a highly useful method of film deposition. Figure 4.1.1 shows a schematic of a magnetron sputtering systems method.

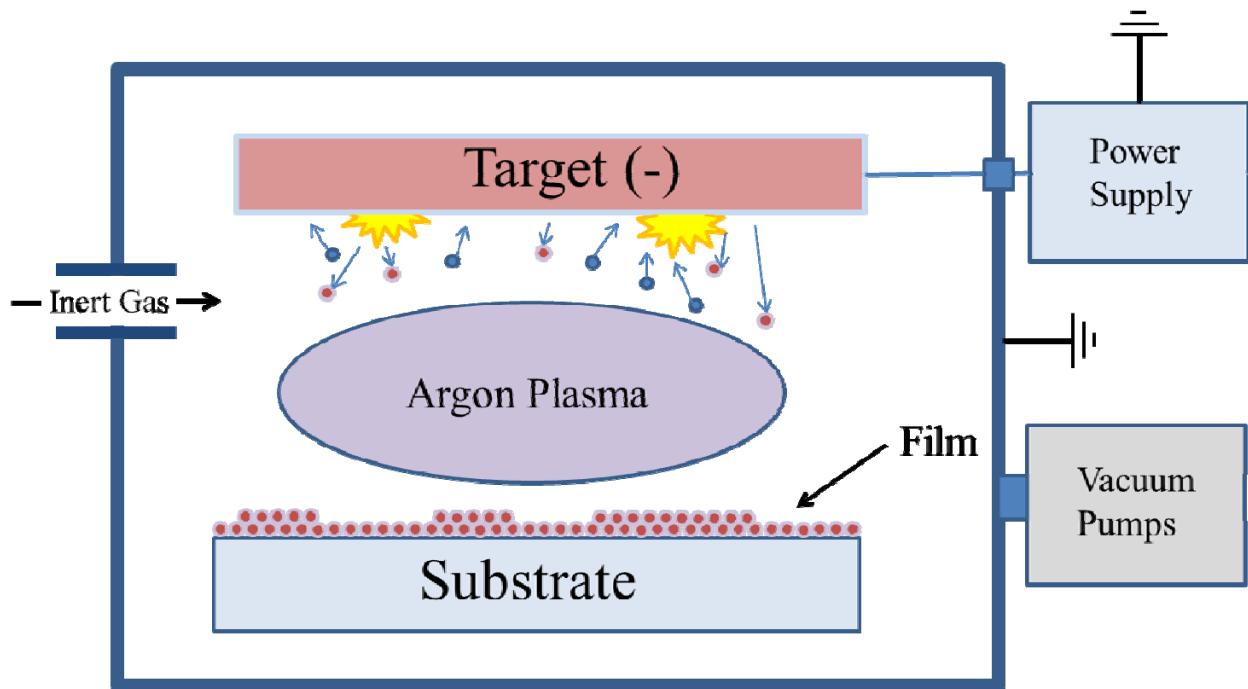


Figure 4.1.1 Schematic of sputtering method

Double side polished substrates of MgO, Si, Al<sub>2</sub>O<sub>3</sub>, Ge and SiO<sub>2</sub>, or Quartz, of 0.5mm thick and 25x25mm or larger and at least 99.99% pure were obtained from MTI Corporation, Richmond, Ca.

Once the substrates were in order, a thin film of gold was to be deposited using a Denton Vacuum Inc. DC & RF magnetron sputtering system, shown in Figure 4.2.1. When depositing films for thin film nanoindentation it is crucial that the films are of uniform quality in terms of surface roughness and depth. To measure the quality of film deposited, the gold was first sputtered onto a cleaned fused silica microscope slide, or SiO<sub>2</sub>. The parameters initially used were extracted from the sputtering system's log book, recorded when gold was previously sputtered by other users when running this system as shown in Table 4.1.1. From these values it was chosen to go with a sputtering power of 100 watts as it was used for the film that most closely resembles the desired thickness of 500nm. To compensate for the original film being



400nm, the sputtering time was increased to 1500 seconds in line with the deposition rate to reach an expected thickness of 500nm.



Figure 4.1.2 Denton Vacuum Inc. DC & RF sputtering system.

Table 4.2.1 Sputtering parameters of 480nm Au film with Ti adhesion layer.

<b>Base Pressure (Torr)</b>	$5 \times 10^{-6}$	
<b>Magnetron Type</b>	<b>DC</b>	<b>DC</b>
<b>Target Material</b>	Au	Ti
<b>Pre-Sputtering Power (W)</b>	100	400
<b>Pre-Sputtering Time (sec)</b>	60	25
<b>Sputtering Power (W)</b>	100	400
<b>Sputtering Time (sec)</b>	1500	25
<b>Gas 1 (Ar) flow rate (sccm)</b>	25	25
<b>Gas 2 (O2/N2) flow rate (sccm)</b>	0	0
<b>Deposition Pressure (mTorr)</b>	4.7	4.7
<b>Deposition Temperature (°C)</b>	23	23
<b>Soak Time (sec)</b>	0	0
<b>Substrate holder rotation (%)</b>	50	50
<b>Ignition Pressure (mTorr)</b>	50	50
<b>Expected Film Thickness (nm)</b>	500	10
<b>Actual Film Thickness (nm)</b>	480	10

After deposition, the film thickness was measured using a Tencor Instruments "Alpha-Step 200" profilometer shown in Figure 4.1.3. For each deposited film, the profilometer's tip was moved across the substrate to film edge in three locations across the tape pull, determining a uniform film thickness of 480nm; 20nm less than expected.



Figure 4.1.3 Tencor Instruments "Alpha-Step 200" profilometer.

## 4.2 Nanoindentation

Nanoindentation was performed using TestWorks 4 to drive an MTS Nanoindenter XP (Agilent Technologies, Santa Clara, CA), as shown in Figure 4.2.1. A Berkovich type diamond tip was used during the experiments in a depth controlled test. The harmonic displacement, or the distance the tip travelled during each oscillation, was set to 2nm and the allowable drift rate of the indenter head was 0.05 nm/s. During each indentation test, twenty five indents were performed on a fused silica reference in order to calibrate the area coefficients of the tip. Next five indents were performed on an aluminum reference material to both clean any debris off of the surface of the indenter and calibrate the position between the camera and indenter head. When setting up the experiment for each film-substrate combination, the value of the bulk film Poisson ratio was input into TestWorks 4. Also, the depth of each indentation test was entered to be 500 nm in order to fully penetrate the film and test the behavior of the film throughout the entirety of the thin film. Twenty five indents were performed on each film-substrate combination in a five by five array separated by 50  $\mu\text{m}$  in both the x and y direction. The average value of the entire array was calculated using the program Analyst and plotted for the composite modulus versus indentation depth for each sample. The data gathered was acquired using the standard Oliver and Pharr analysis.

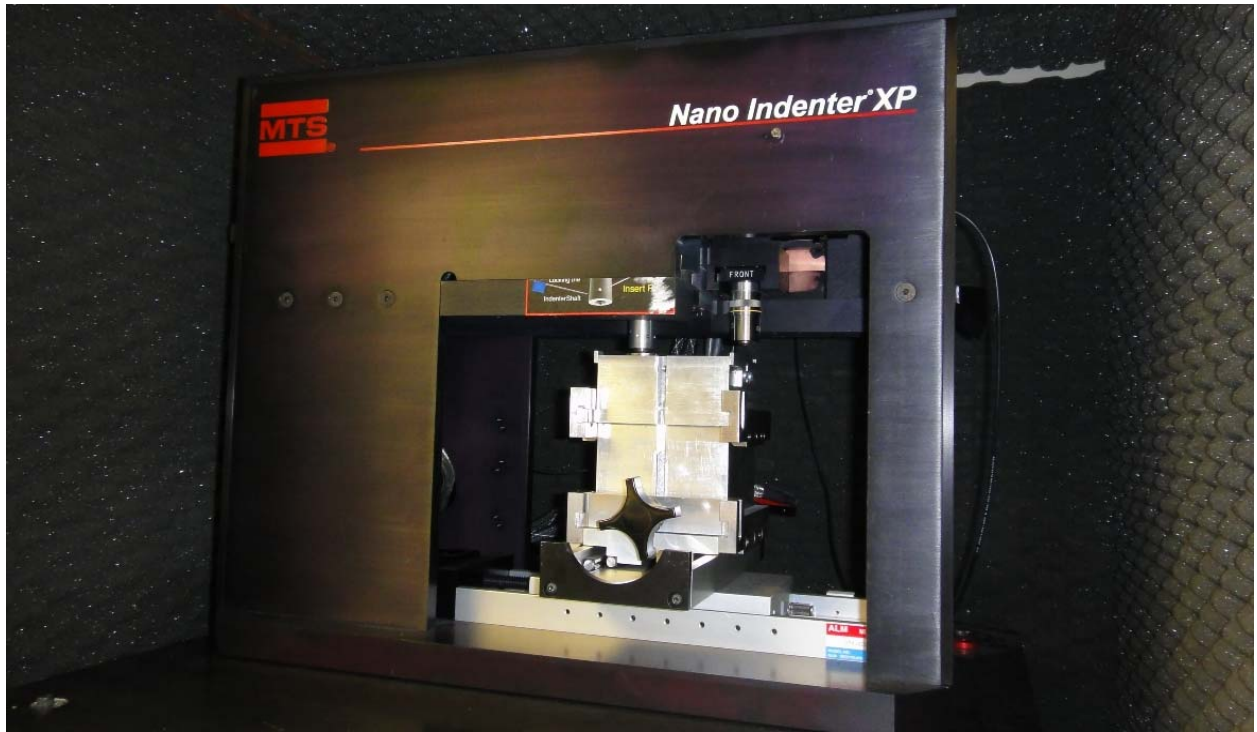


Figure 4.2.1 Image of MTS Nano Indenter XP nanoindentation system.

## Chapter 5: Results and Discussions

### 5.1 Experimental Nanoindentation Analysis

Before running any indentation tests, the discontinuous model was examined to determine what changing various film and substrate properties would result in. Figures 3.1.1-3.1.5 show  $E-h$  curves of arbitrary films on substrates with varying film moduli and Poisson ratios. Figure 3.1.1a shows that as the substrate modulus is held constant at 100 GPa, changing the film's modulus results in an increase or decrease in the composite modulus upon further indentation depth with decreasing or increasing substrate modulus respectively. The trends of the composite moduli suggest that the substrate effect on the composite modulus increases upon further indentation depth. When varying the substrate modulus, the effect of the composite modulus was inverted. As the substrate modulus was increased, relative to that of the film's modulus, the resulting composite modulus trend line increased upon further indentation depth and vice versa.

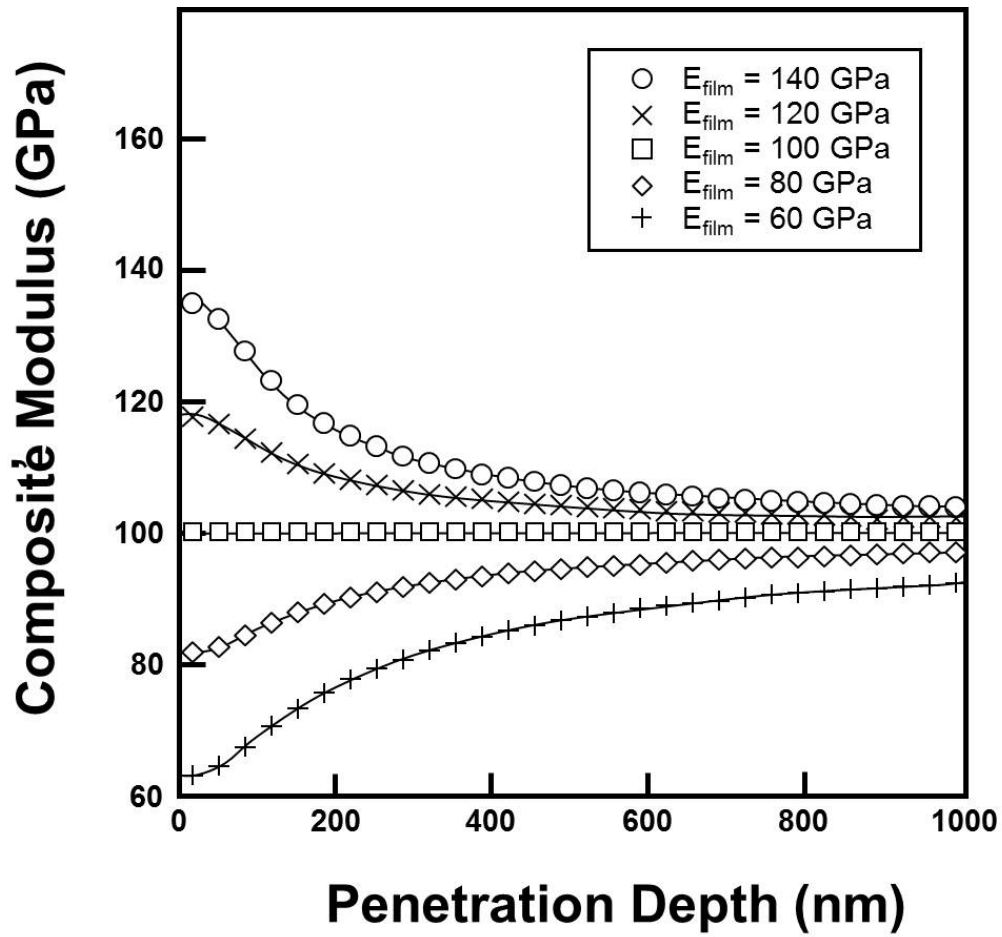


Figure 5.1.1  $E$ - $h$  curve of arbitrary film on substrate with varying film modulus

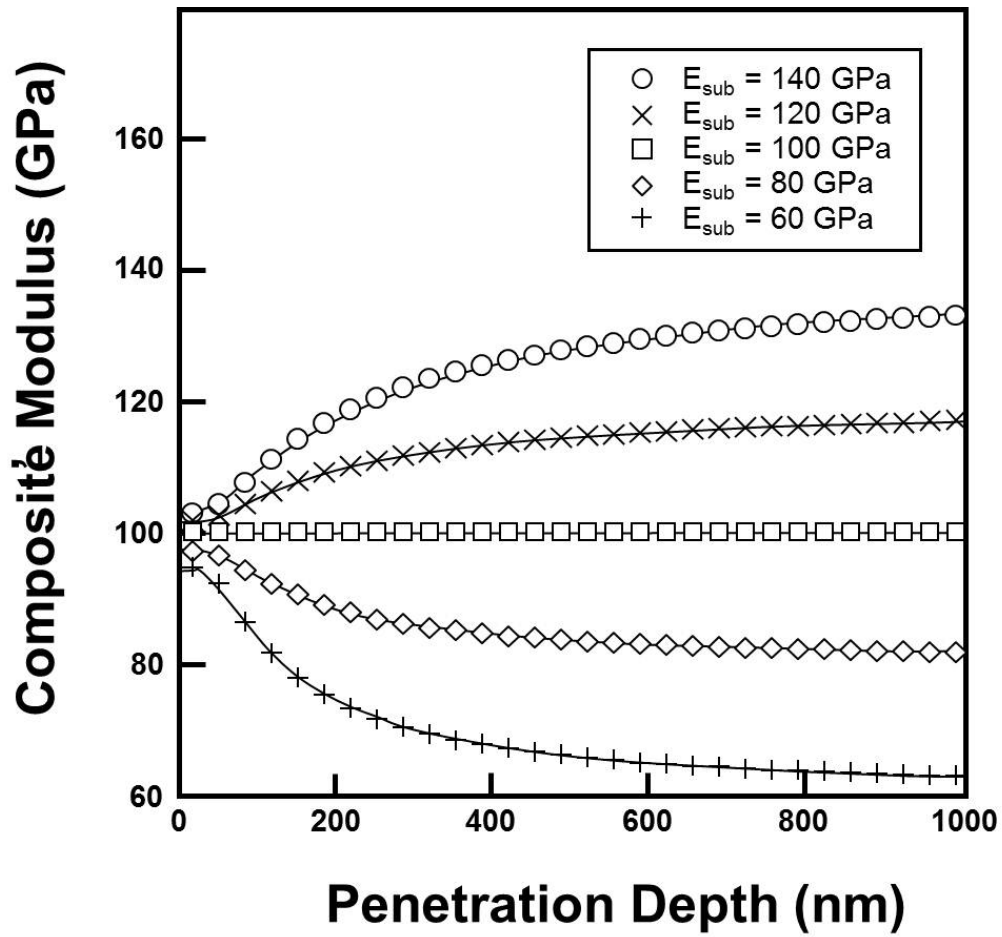


Figure 5.1.2  $E-h$  curve of arbitrary film on substrate with varying substrate modulus



After varying the film and substrate's moduli with respect to each other, the Poisson's ratios were changed to observe the resulting trends. Figure 3.1.3 shows that keeping all the parameters constant while varying the film's Poisson ratio resulted in an initial increase or decrease in composite modulus. A film with a Poisson ratio of 0.50 on a substrate having a Poisson ratio of 0.30 resulted in an increase of the composite modulus at first but leveled off to that of the substrate's modulus upon further indentation depth. Conversely, a film with a Poisson ratio of 0.10 on a substrate with a Poisson's ratio of 0.30 results in a dip in the composite modulus and approaches the substrate's modulus eventually. In Figure 3.1.6, it was seen that as the differences in the film and substrate's Poisson ratios became increasingly far apart, the effect of the increase in composite modulus was intensified. The expected behavior of the gold film on a  $\text{SiO}_2$  substrate can be seen in figure 3.1.6 where the Poisson ratios of the two are very different. According to the discontinuous theory, the film with a Poisson ratio of 0.44 "wants" to spread out during compression while the  $\text{SiO}_2$  substrate with a Poisson ratio of 0.18 shows minimal displacement in the z and y direction, thus resulting in a temporary increase in the composite modulus. The increase in the composite modulus arises from the substrate restricting the expansion of the film during the indentation test.

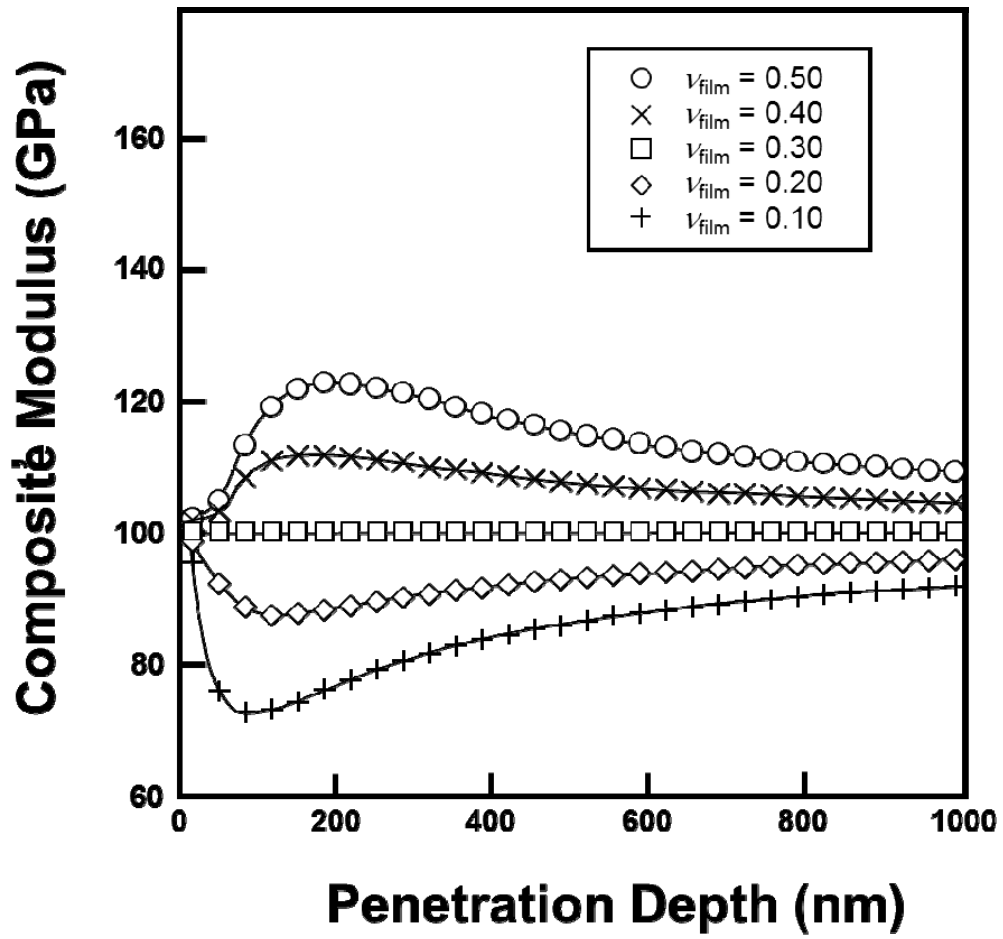


Figure 5.1.3  $E-h$  curve of arbitrary film on substrate with varying film Poisson ratio

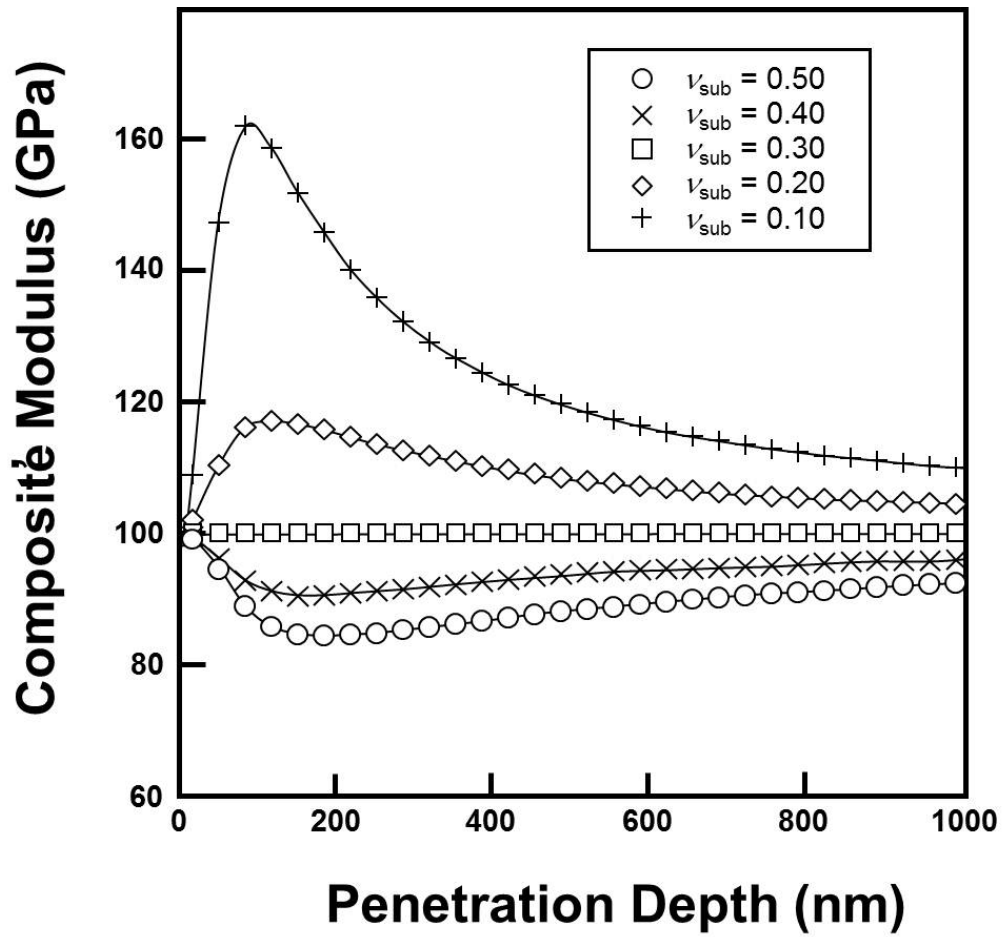


Figure 5.1.4  $E-h$  curve of arbitrary film on substrate with varying substrate Poisson ratio

The combined effect of changing the substrate and film Poisson ratios is shown in Figure 5.1.5. Here, it can be seen that as the differences in Poisson ratios increase, the substrate effect becomes larger.

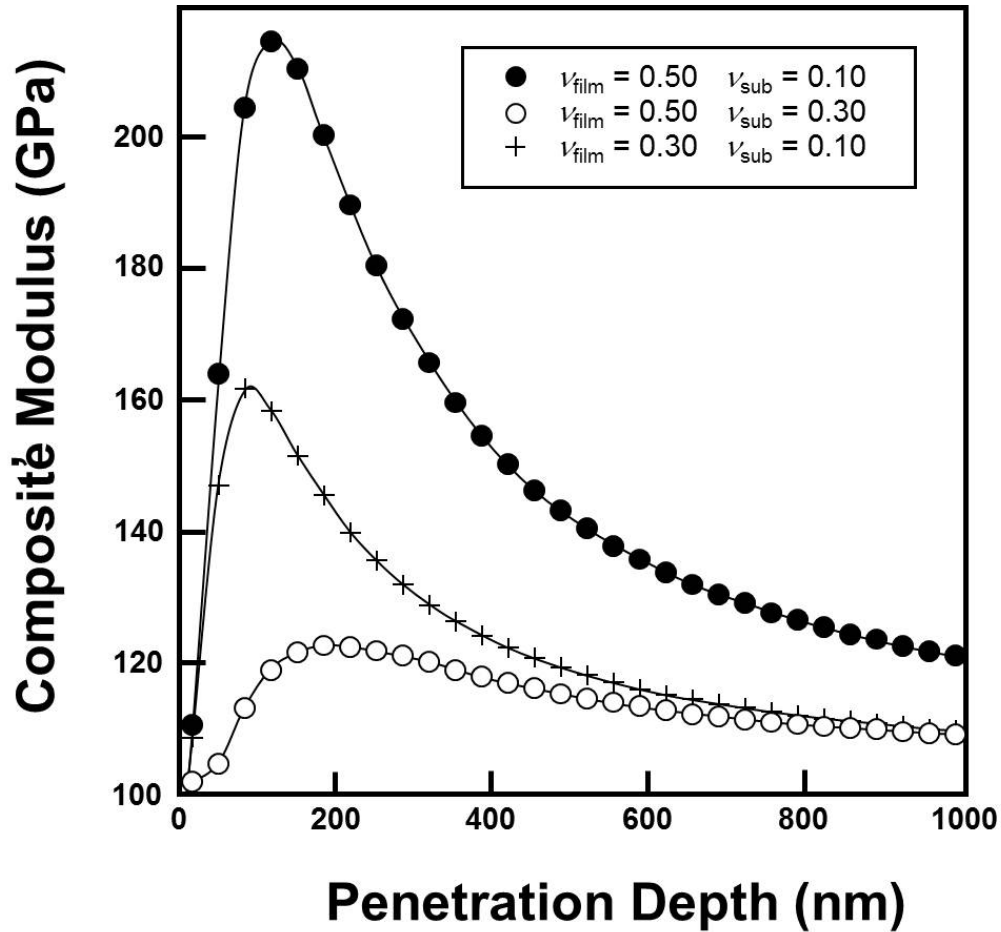


Figure 5.1.5 *E-h* curve of arbitrary film on substrate showing combined effect of varying Poisson ratios of film and substrate

Nanoindentation tests at indentation depths of 500nm were performed on substrates  $\text{Al}_2\text{O}_3$ , MgO, Ge, Si and  $\text{SiO}_2$  in order to get the values of the bulk moduli. These tests were

performed in order to get the actual values of the substrates Young's moduli rather than referring to the literature for the reported moduli, since the values could be slightly different due to various factors such as crystal orientation.

Raw CSM Nanoindentation data of all the film substrate combinations were put into Analyst software, which is a program used with the MTS-Nano Nanoindenter XP system to process the data. The Analyst software calibrated the data from each CSM test. The results showed a horizontal line throughout the indentation tests representing the bulk moduli of the substrates. At very low indentation depths, the measured values were lower than that of the values at deeper depths due to the indenter tip initially losing contact with the surface of the substrate during the tip oscillation of the CSM method. Figures 5.1.6a-e show the results of the indentation tests on the five substrates. It should be noted that the data for the SiO<sub>2</sub> substrate indentation test showed a slight variation at lower indentation depths eventually leveling out at larger depths.

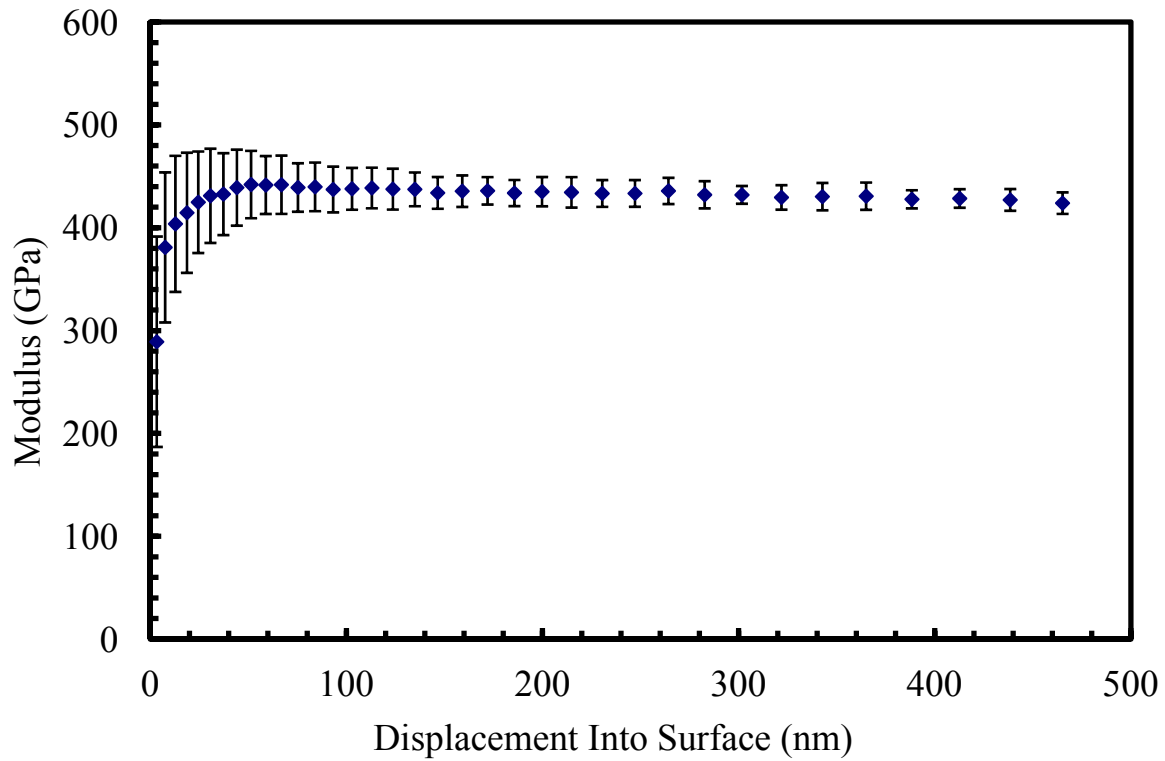


Figure 5.1.6a *E-h* curve for Al<sub>2</sub>O<sub>3</sub> substrate.

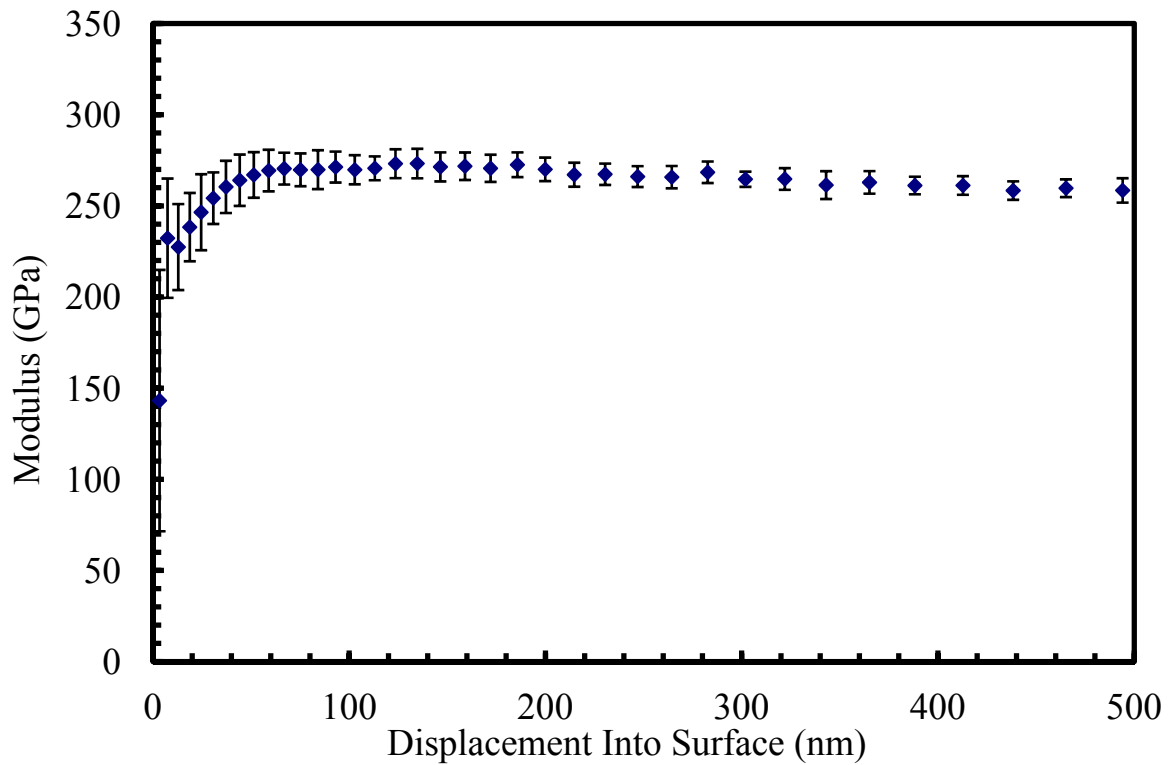


Figure 5.1.6b *E-h* curve for MgO substrate.

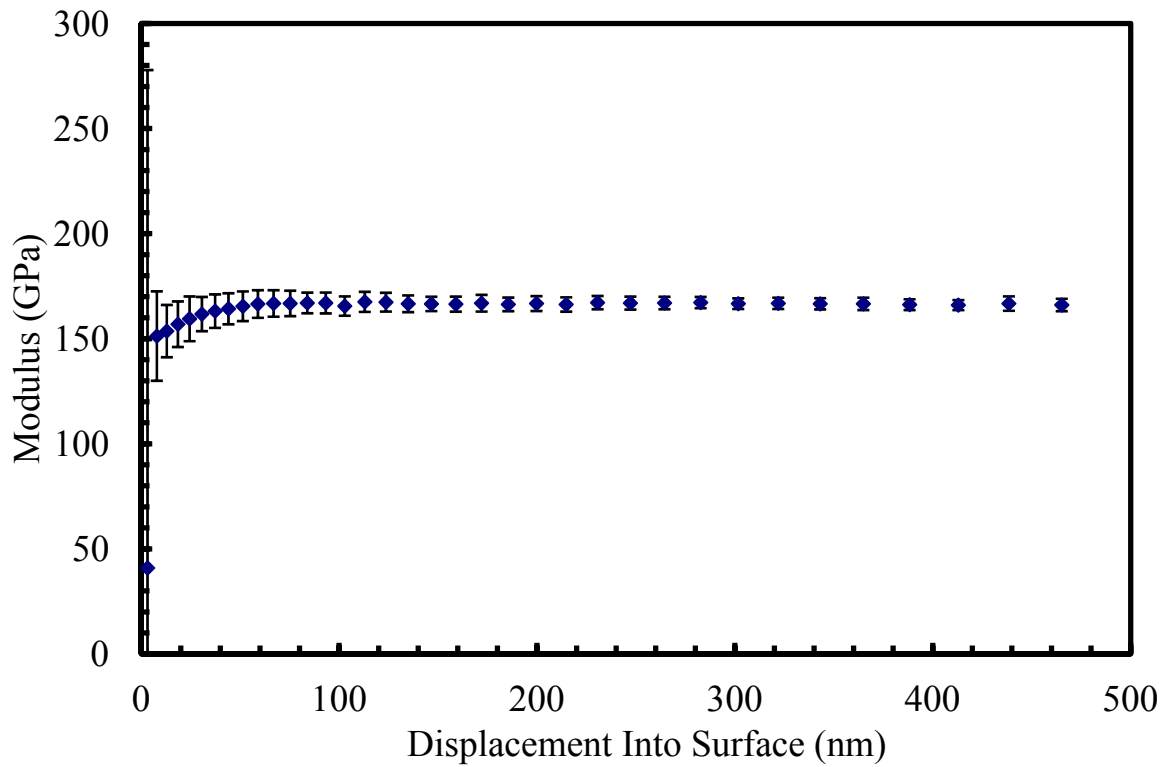


Figure 5.1.6c E-h curve for Si substrate.

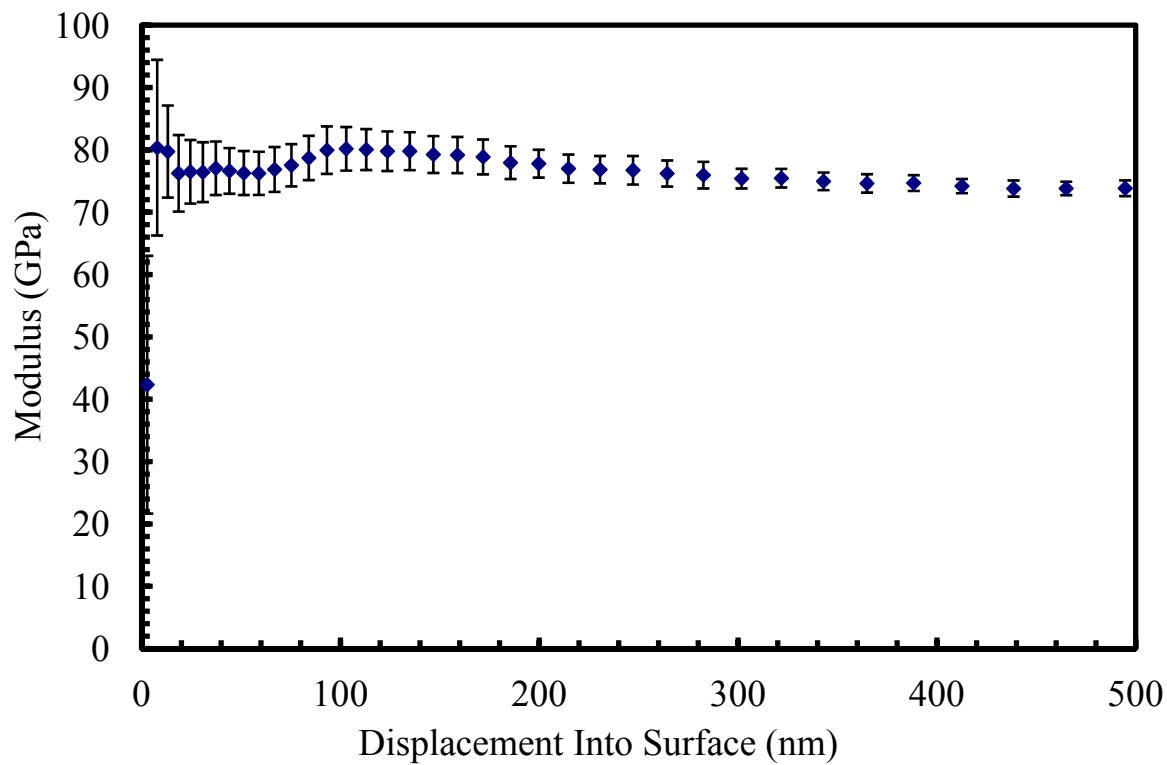


Figure 5.1.6d E-h curve for SiO<sub>2</sub> substrate.

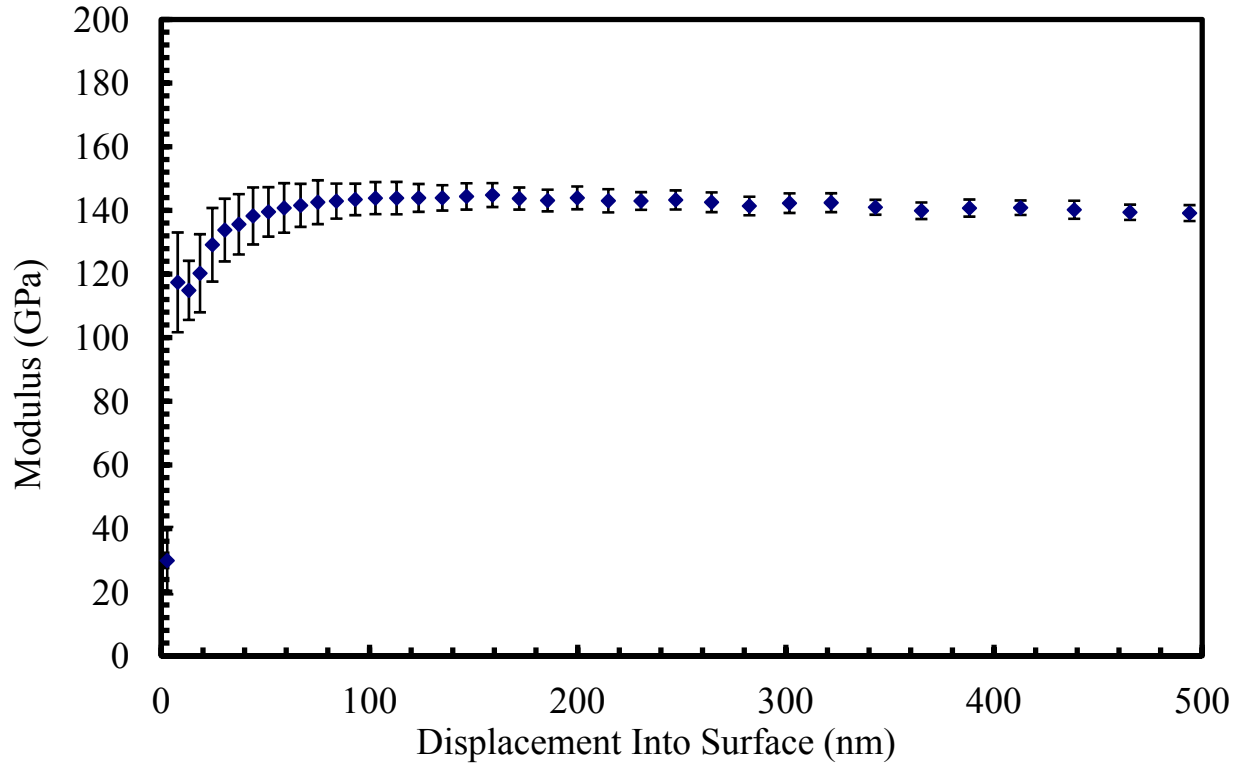


Figure 5.1.6e E-h curve for Ge substrate.

After the substrates were indented on, and it was known how they would behave with a film on them, the substrates were indented with Au films on them. Figure 5.1.7 shows the composite modulus versus displacement for all five film-substrate combination. The results of the indentation tests agree with the previous graphs of varying Young's moduli and Poisson's ratios. Figures 5.1.8 -5.1.15 show  $E-h$  curves of the data for each substrate along with several other areas of interest including the discontinuous model from equation (12), the Doerner and Nix model from equation (8), the extracted film's Young's modulus from equation (12) and the film alpha, or film Poisson ratio, extracted from equation (10). The Doerner and Nix model was added in order to compare the fit with the composite modulus data to that of the discontinuous model. From the figures, it is noteworthy to add that the degree of flatness of the extracted film alpha and Young's modulus is an indication of how well the data matched the model. In several



cases, the film's alpha would start out at lower or higher values than expected and eventually level out to the correct values as the indenter went further into the film. The reason for the deviation at first could be due to indenter losing contact with the film at first and recording errant stiffness values, which would then translate to higher or lower Young's moduli.

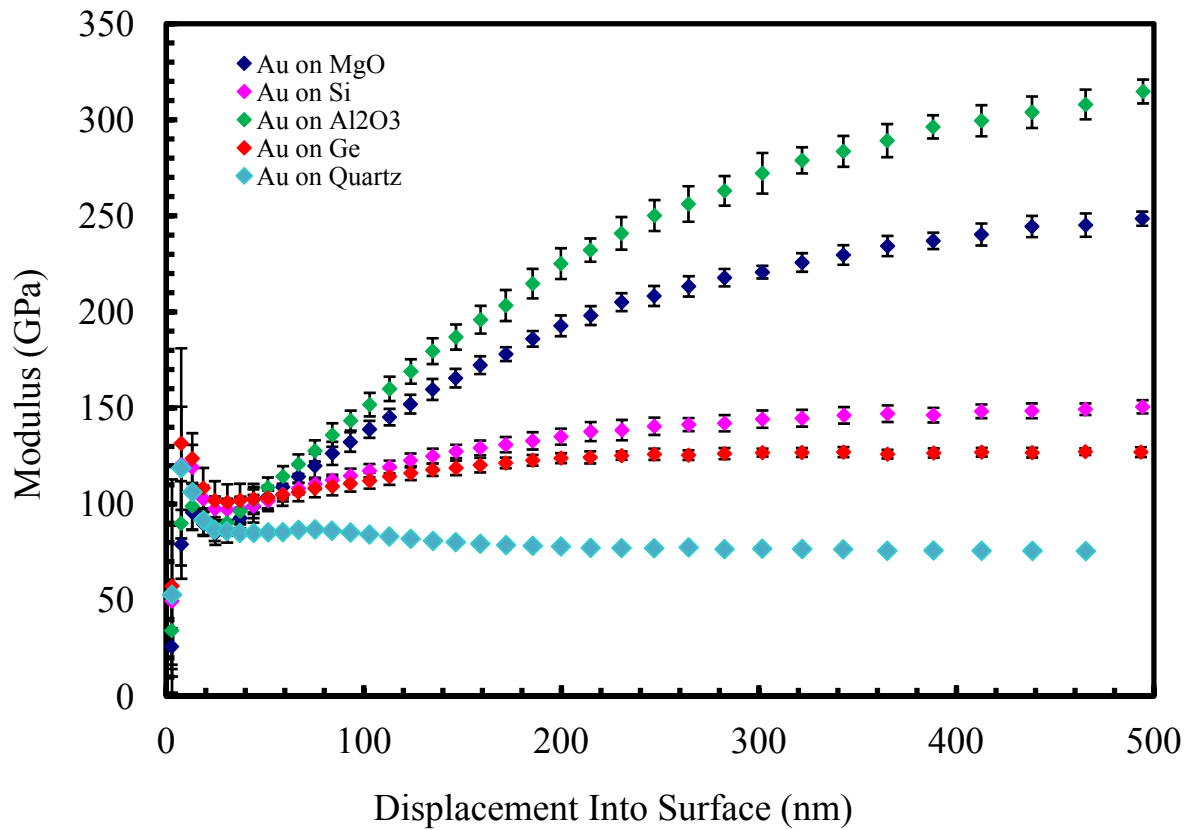


Figure 5.1.7 E-h curve for Au on 5 different substrates.

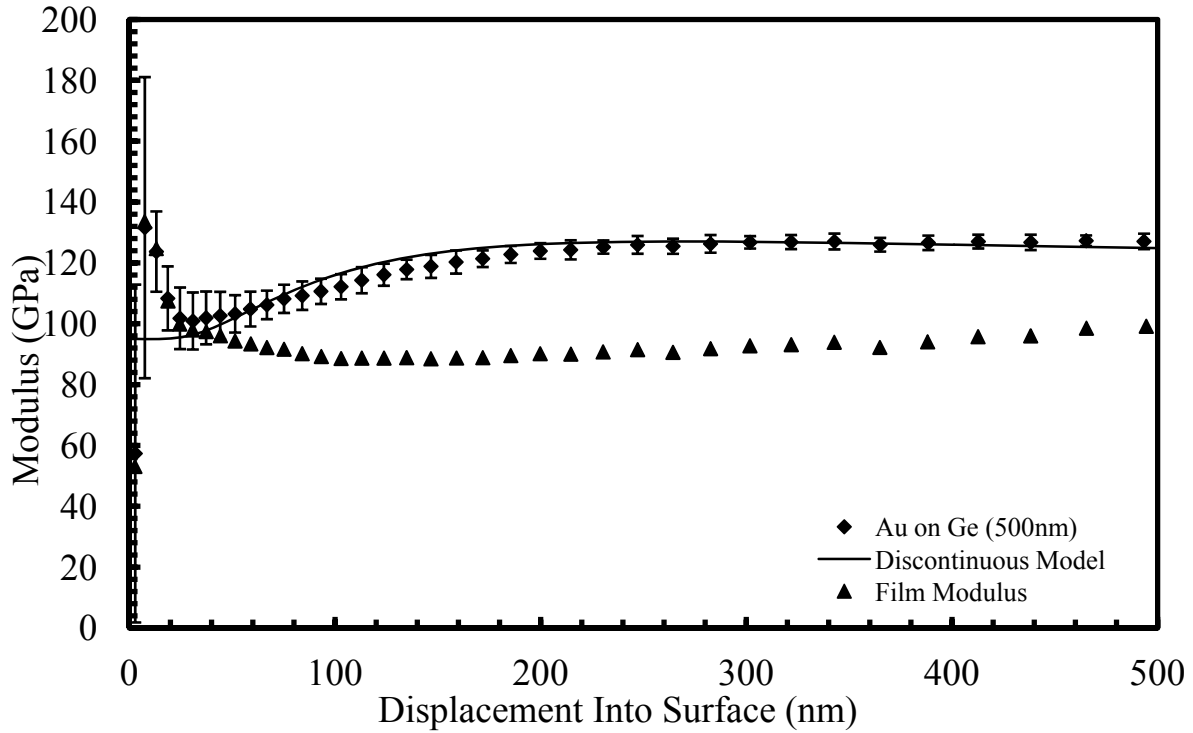


Figure 5.1.8  $E-h$  curve with discontinuous model and film  $E$  for 500nm Au on Ge with Ti adhesion layer.

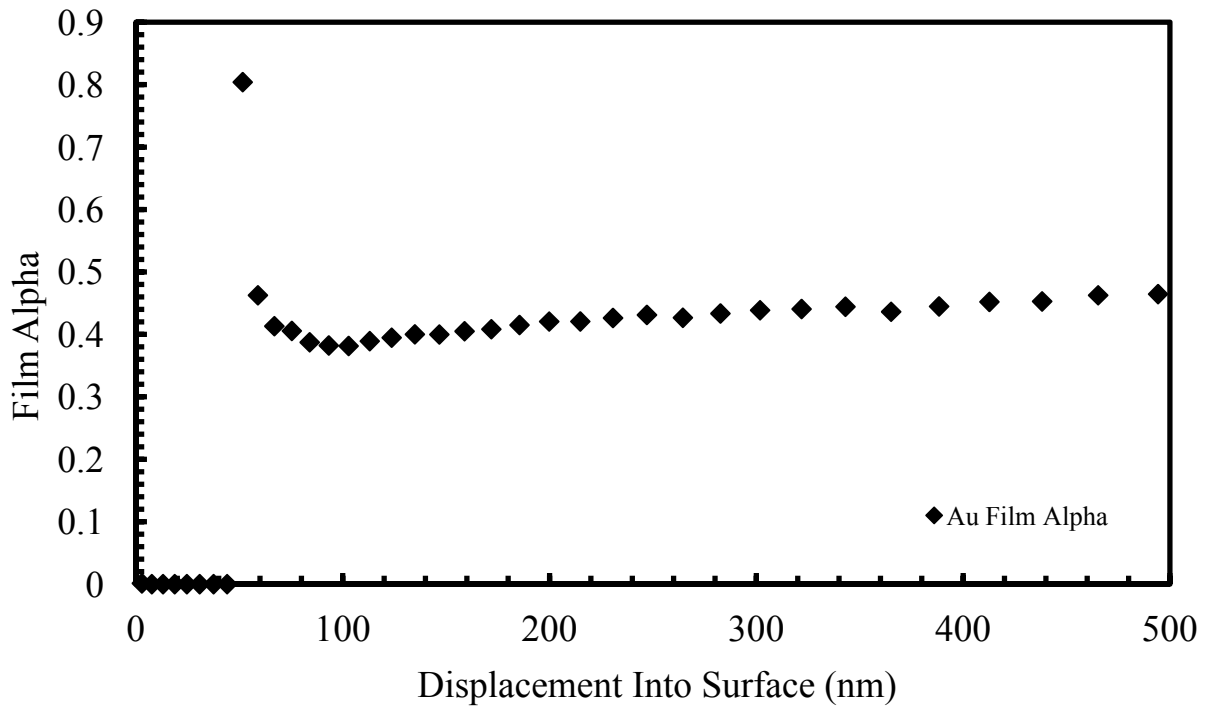


Figure 5.1.9  $\alpha-h$  curve for 500nm Au on Ge with Ti adhesion layer.

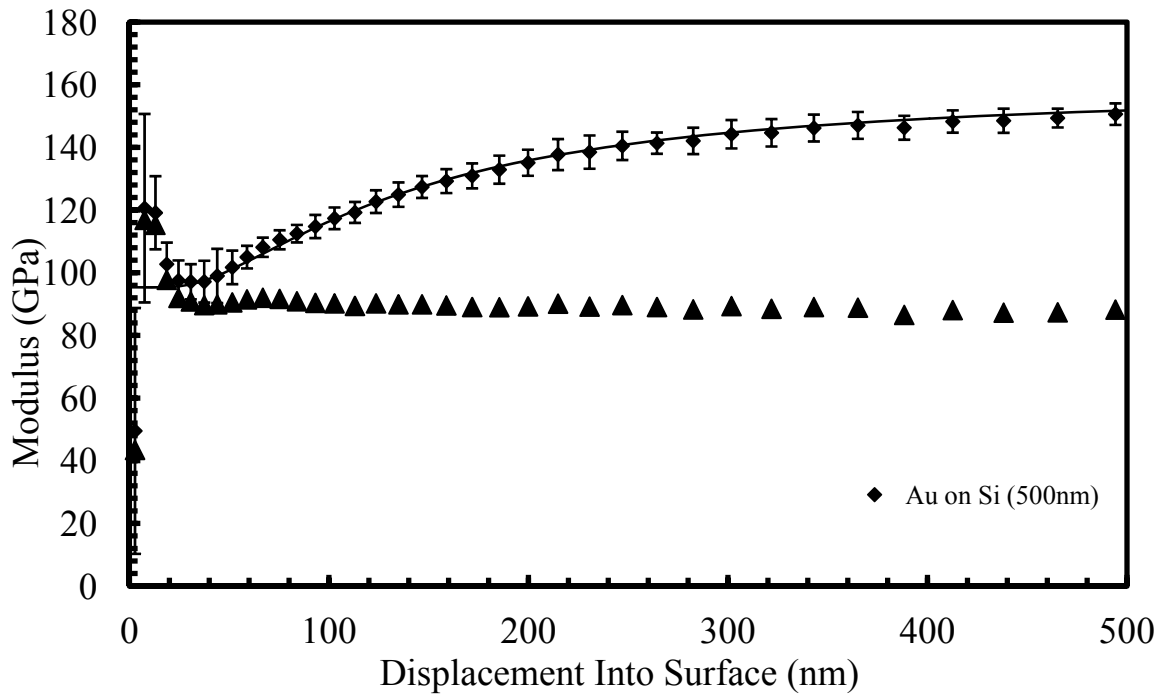


Figure 5.1.10  $E-h$  curve with discontinuous model and film E for 500nm Au on Si with Ti adhesion layer.

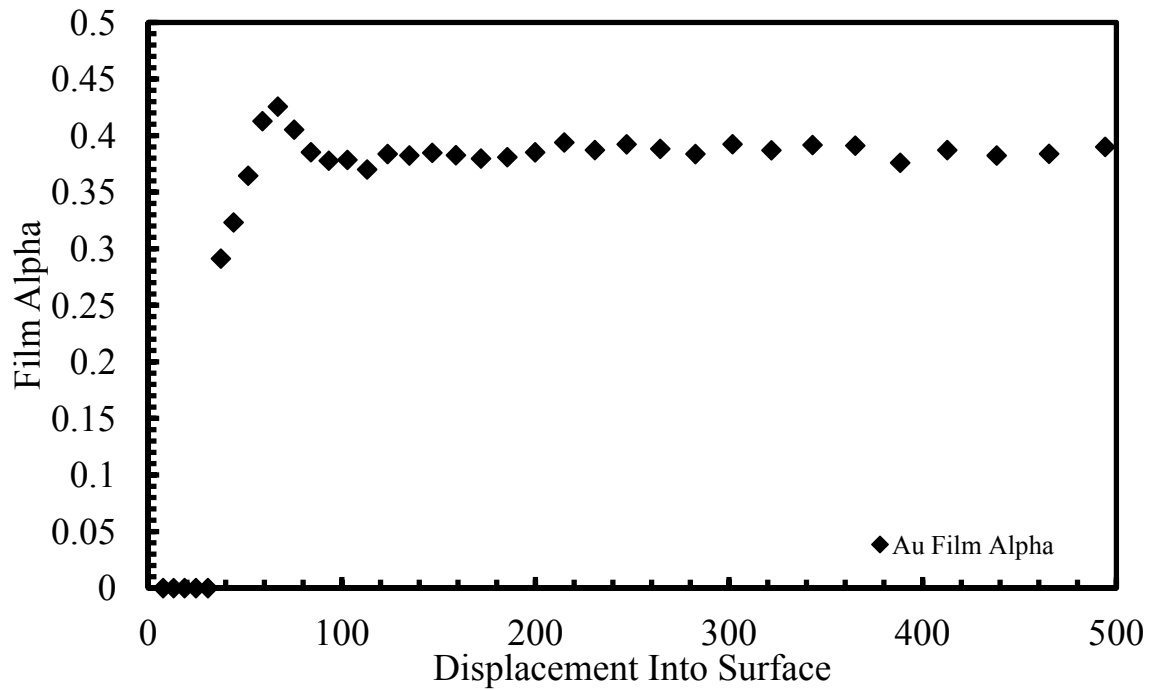


Figure 5.1.11  $\alpha-h$  curve for 500nm Au on Si with Ti adhesion layer.

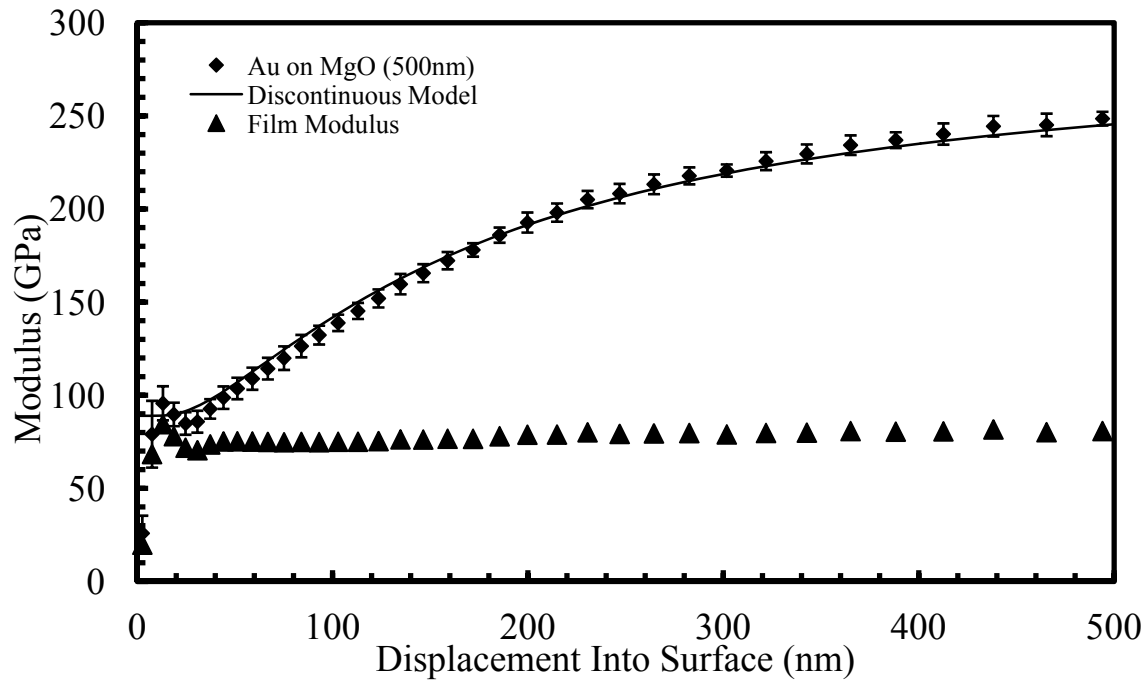


Figure 5.1.12  $E-h$  curve with discontinuous model and film E for 500nm Au on MgO with Ti adhesion layer.

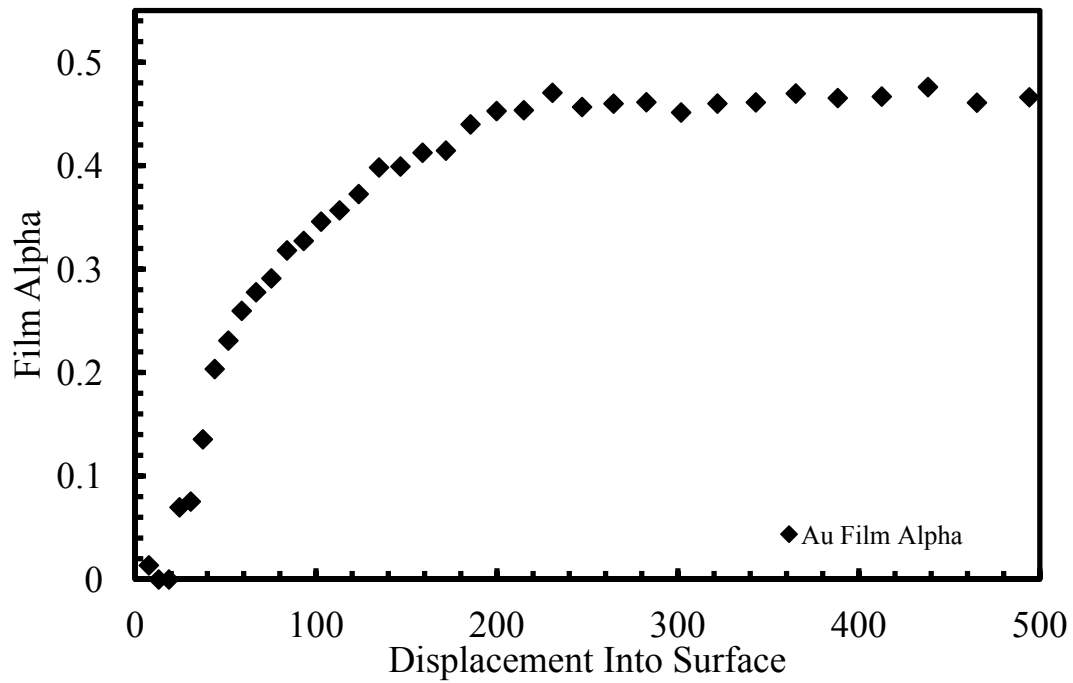


Figure 5.1.13  $\alpha-h$  curve for 500nm Au on MgO with Ti adhesion layer.

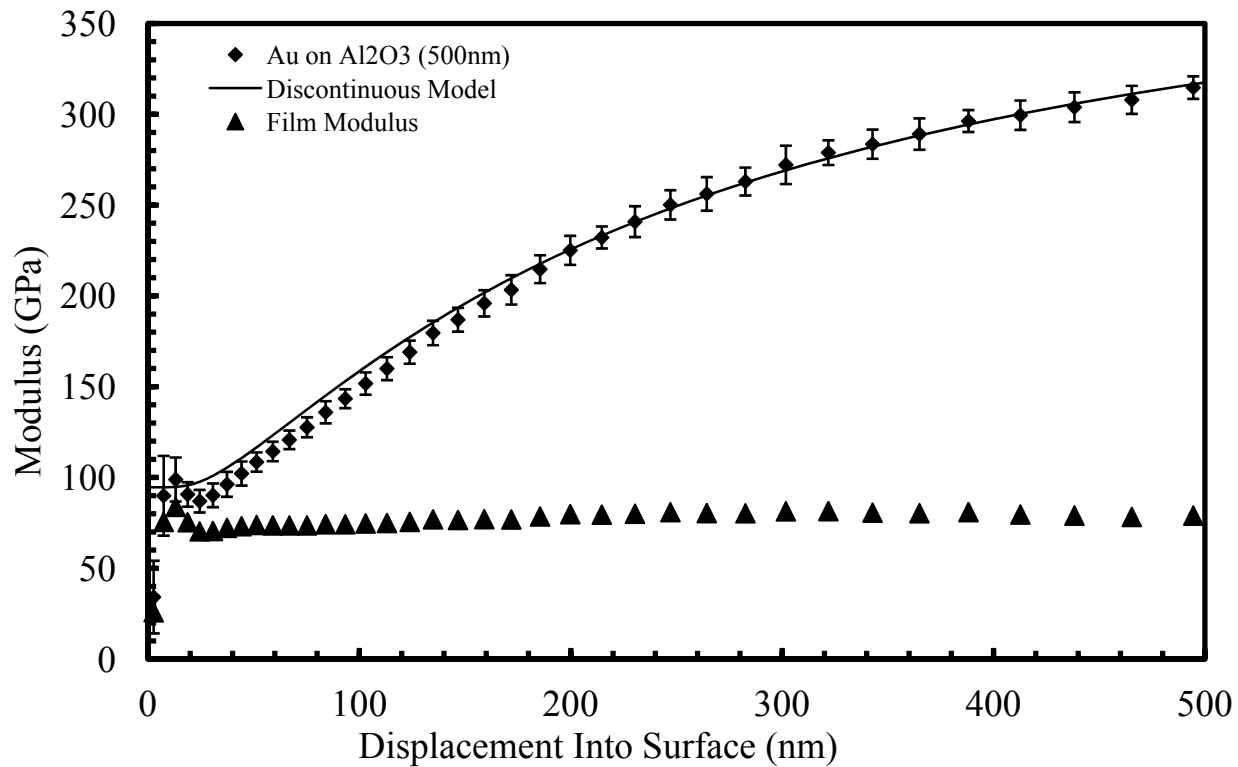


Figure 5.1.14  $E-h$  curve with discontinuous model and film E for 500nm Au on  $\text{Al}_2\text{O}_3$  with Ti adhesion layer.

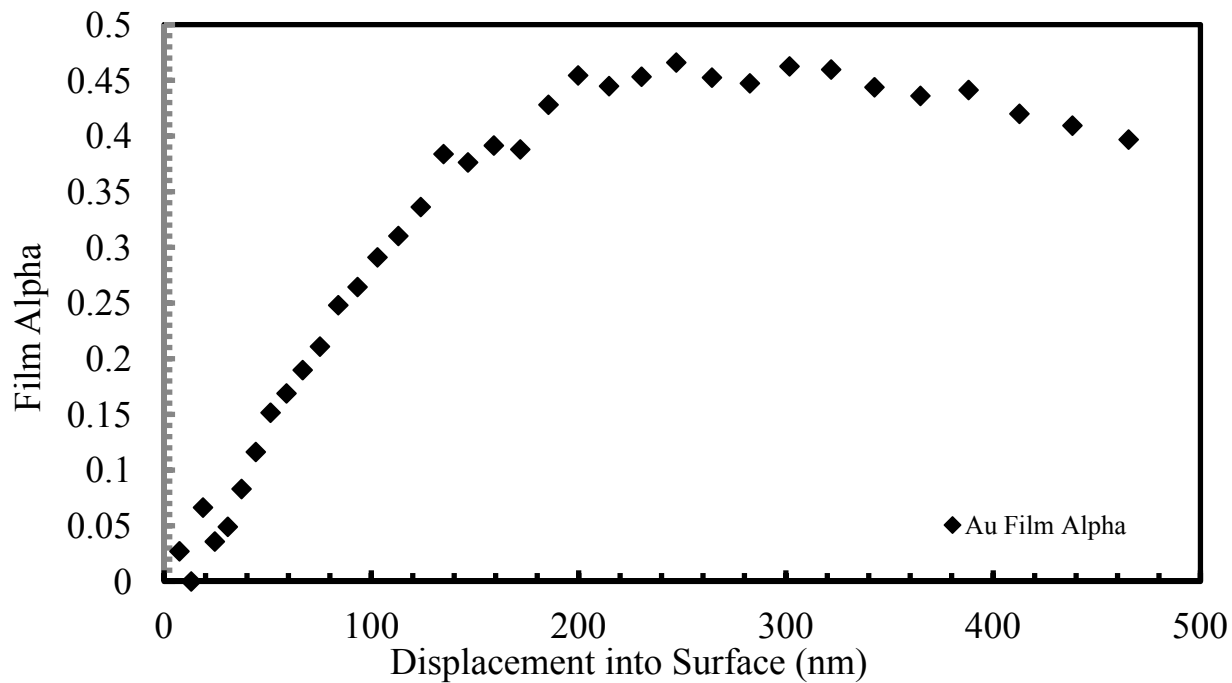


Figure 5.1.13  $\alpha-h$  curve for 500nm Au on  $\text{Al}_2\text{O}_3$  with Ti adhesion layer.

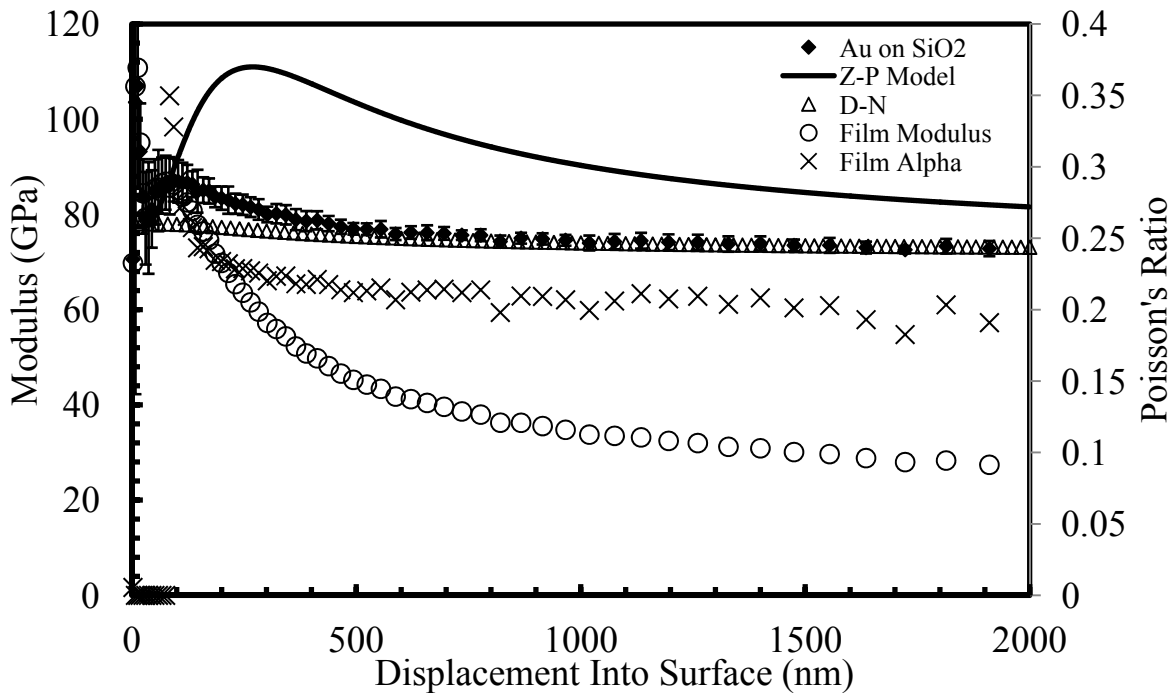


Figure 5.1.15 E-h curve with Z-P model, film E, and film alpha for 2000nm Au on SiO<sub>2</sub>.

In order to get a better picture of how the models matched the data for SiO<sub>2</sub>, A plot of an *E-h* curve is shown in 5.1.16. Here, it can be seen that the data matched the discontinuous model early on but then dropped back down to what the D-N model would predict. The composite modulus increased with indentation depth at shallow indentation depths higher than the bulk modulus of SiO<sub>2</sub> or the Au film, and then rapidly decreased to the value of the substrates modulus. Due to the fact that Au and SiO<sub>2</sub> have similar Young's moduli but different Poisson ratios, the behavior of the composite modulus is greatly affected by the Poisson ratio mismatch. As the indenter penetrates deeper into the film surface, the Au thin film should spread out as described by the films Poisson ratio of 0.44. However, the substrate has a Poisson ratio of 0.18 which is much lower than that of Au. The discontinuity in the Poisson ratio would suggest that

the lateral movement of the film material upon loading should be restricted by the relatively low ratio of the substrate. This behavior would suggest that the film could be losing adhesion with the substrate and delaminating from the substrate.

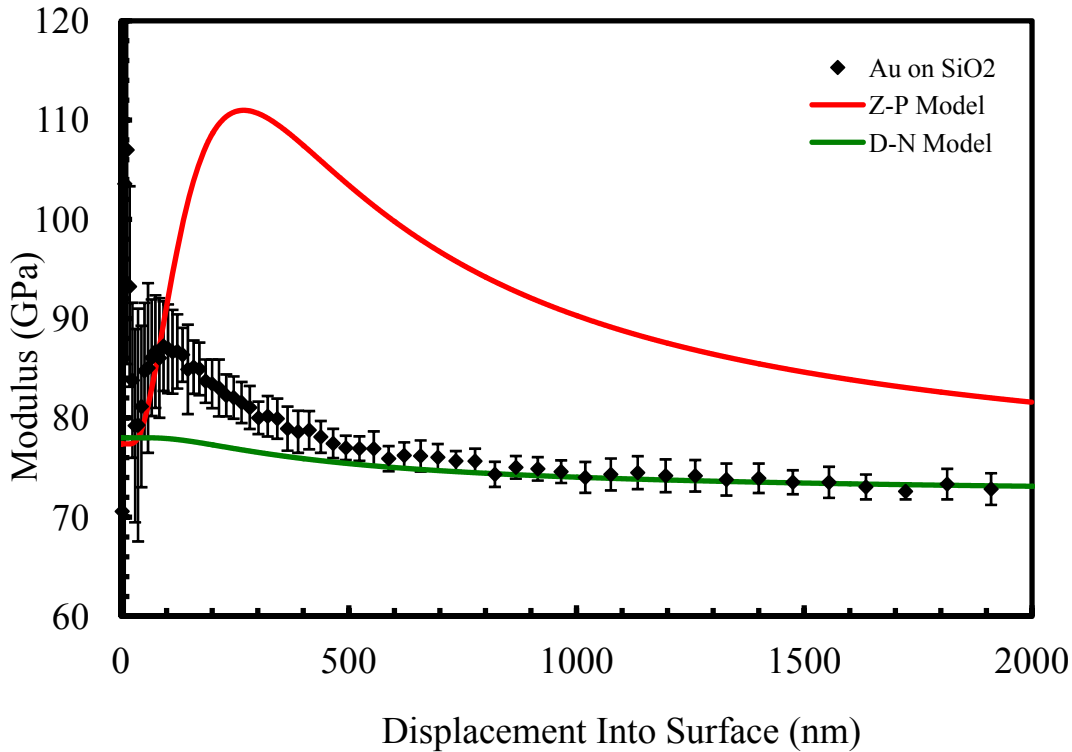


Figure 5.1.16 E-h curve with discontinuous model and D-N model for 2000nm Au on SiO<sub>2</sub>.

From the previous results from the Au film on SiO<sub>2</sub>, micrographs of the indents were necessary to understand how the film was behaving during indentation. A JEOL JSM 7000F Scanning Electron Microscope was used to gather images of indents on various indentation depths of Au on SiO<sub>2</sub>. Figure 5.1.17 shows a picture of the scanning electron microscope used to image the indents.



Figure 5.1.17 JEOL JSM 7000F Scanning Electron Microscope.

Images of Au films of on  $\text{SiO}_2$  are shown in figures 5.1.18 – 5.1.23. The thickness of the Au film was approximately 2000nm and indents were made at depths of 370nm, 500nm, 800nm, 1000nm, 1500nm and 1700nm. From the images, it can be seen that as the indenter went deeper into the film, the amount of pile-up around the indenter increased. At the relatively shallow depth of 370nm, the bowing around the edge of the indenter profile is minimal. However, as the indentions were made at progressively larger depths the bowing around the tip increased.



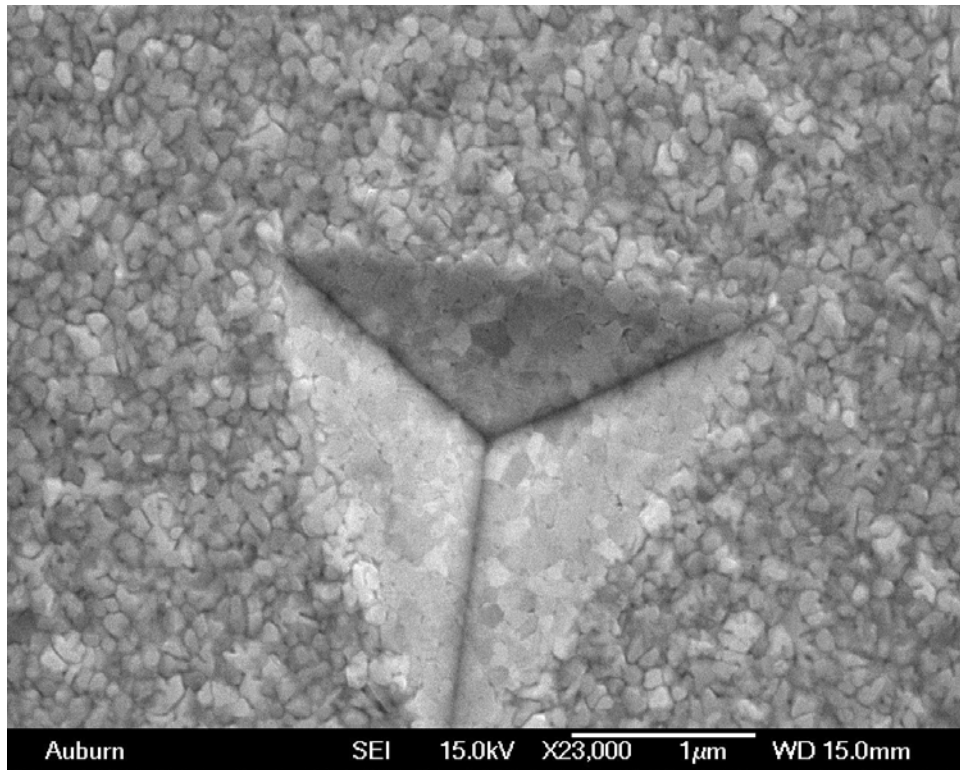


Figure 5.1.18 Micrograph of 2000nm Au on SiO<sub>2</sub> 370nm indentation

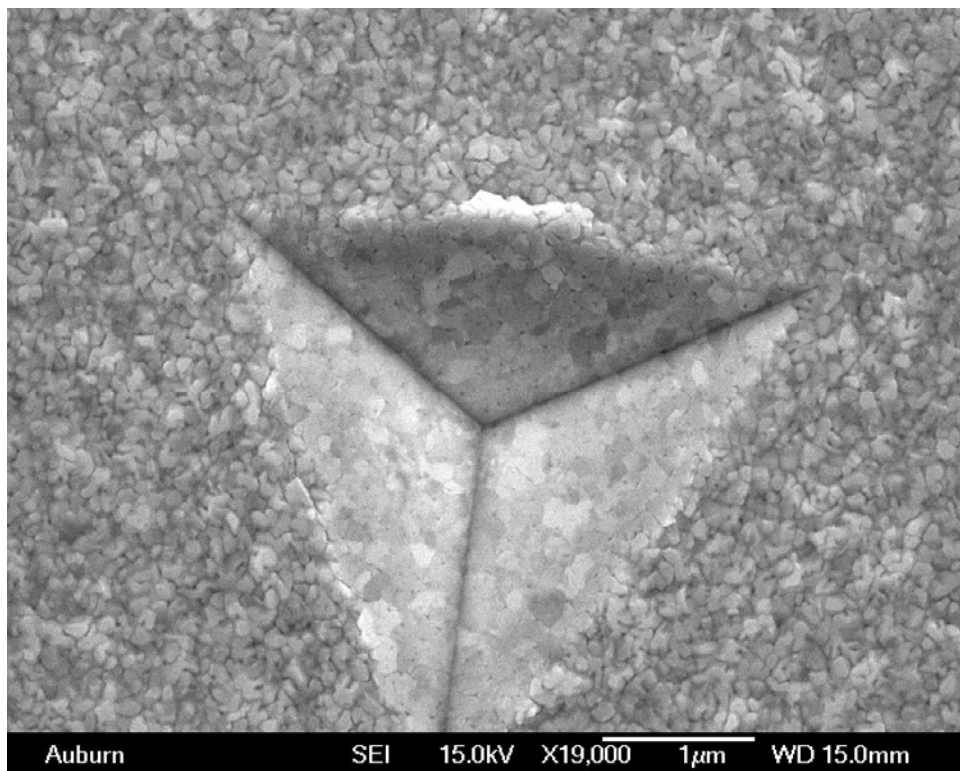


Figure 5.1.19 Micrograph of 2000nm Au on SiO<sub>2</sub> 500nm indentation

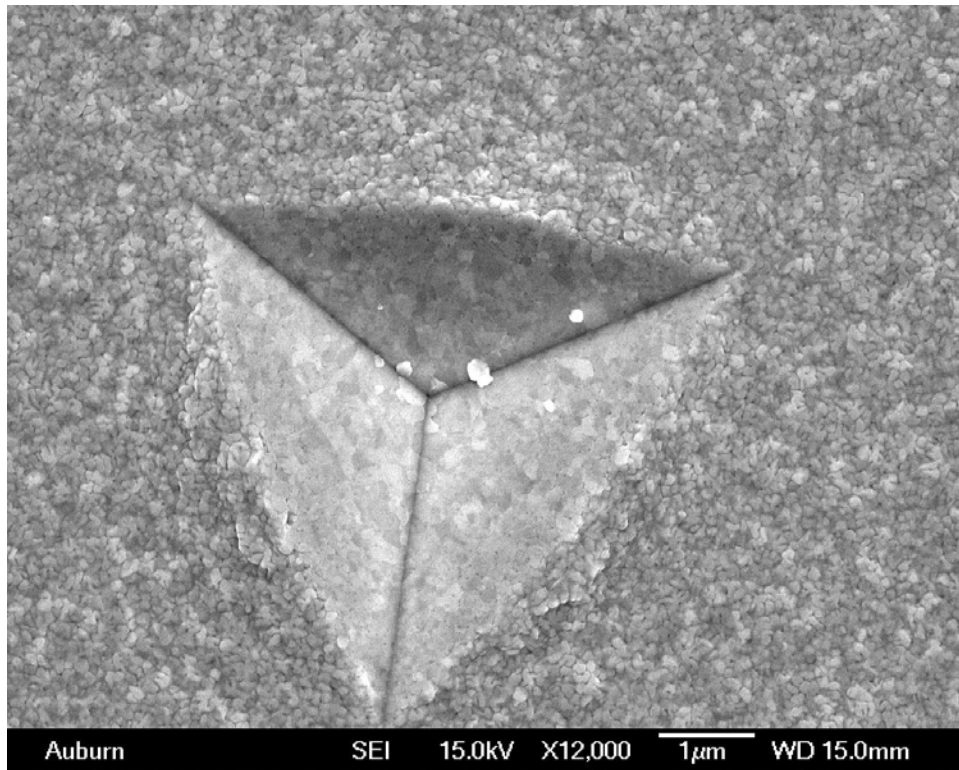


Figure 5.1.20 Micrograph of 2000nm Au on SiO<sub>2</sub> 800nm indentation

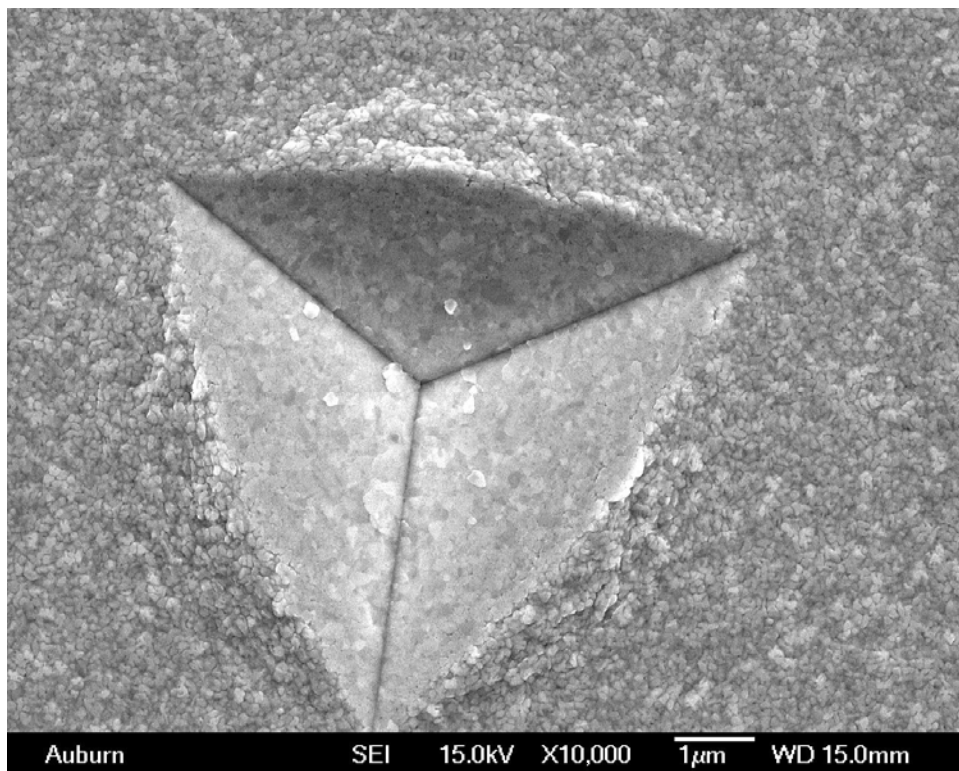


Figure 5.1.21 Micrograph of 2000nm Au on SiO<sub>2</sub> 1000nm indentation

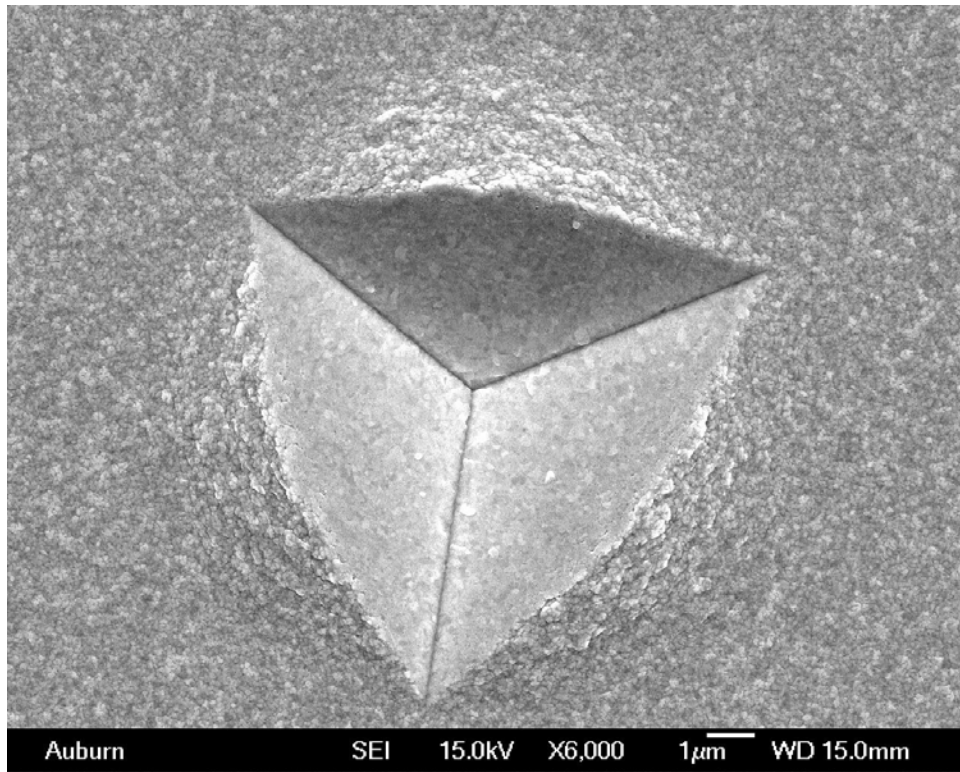


Figure 5.1.22 Micrograph of 2000nm Au on SiO<sub>2</sub> 1500nm indentation

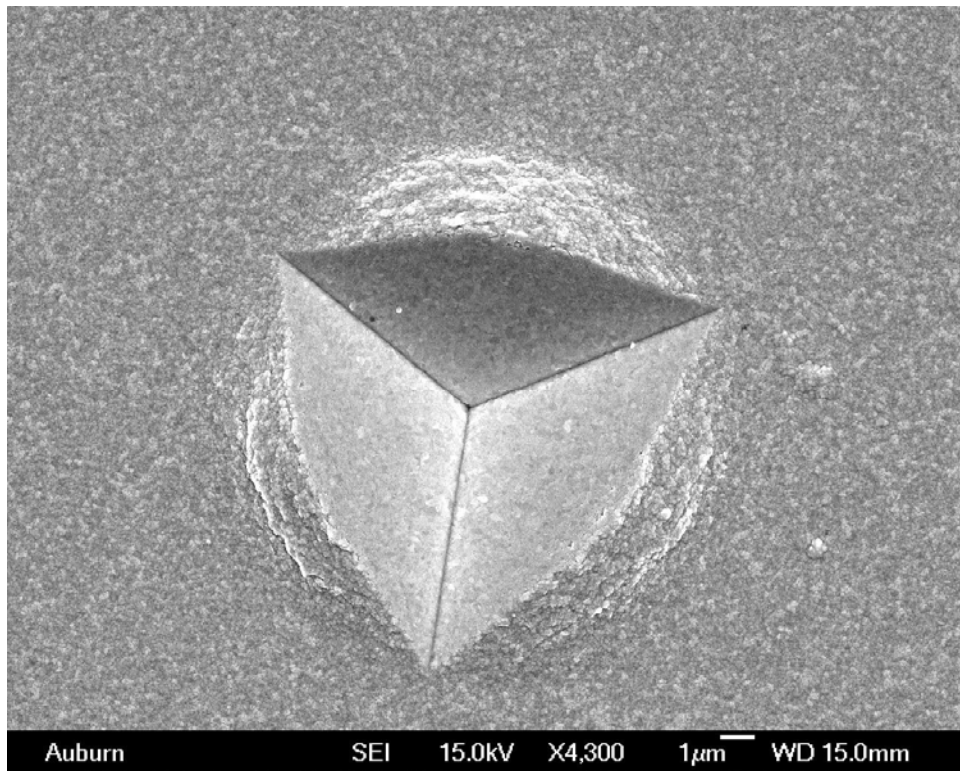


Figure 5.1.23 Micrograph of 2000nm Au on SiO<sub>2</sub> 1700nm indentation

## Chapter 6: Conclusions

Nanoindentation was used to investigate the substrate effect of five different substrates,  $\text{Al}_2\text{O}_3$ ,  $\text{MgO}$ ,  $\text{Ge}$ ,  $\text{Si}$  and  $\text{SiO}_2$  with the same Au film on each one. The CSM method was used in the Nanoindentation experiments to acquire Young's modulus versus indent depth for each film-substrate combination. Sputtering was used in order to achieve 500 nm nanocrystalline Au thin films on each substrate. Upon running the indentation experiments on each film-substrate combination, the resulting composite modulus versus indent depth curves were compared to the discontinuous model to confirm the effect of the substrate on the composite modulus. When comparing the data with the model, the film's modulus and Poisson ratio was extracted to determine how well the experimental data fit the theoretical prediction by looking at what degree the two parameters remained constant throughout the tests.

Upon comparing the experimental data with the model, it was found that the model was able to predict the composite modulus quite well for Au on  $\text{Al}_2\text{O}_3$ ,  $\text{MgO}$ ,  $\text{Ge}$  and  $\text{Si}$ . The extracted film modulus and Poisson ratio also remained flat through most of the indentation tests, which would suggest that the model fit with the data. However, in the case of Au on  $\text{SiO}_2$ , the discontinuous model suggests that there should be an increase in the composite modulus initially, which the experimental data did not coincide with. The Au film on  $\text{SiO}_2$  did exhibit a small increase in composite modulus at first, but quickly dropped back down to that of the substrate's bulk modulus. Upon further indentation depth, the behavior of the film-substrate combination returned to what the Doerner and Nix single alpha model predicted. It was concluded that Au film experienced delamination during indentation just after a very shallow depth. The delamination of the film resulted in the discontinuity at the interface not restricting the total strain of the film on the substrate and thus the experimental composite modulus was not as high

as expected after the initial indent depth. SEM micrographs were taken of the indents to see the morphology of the indents. In the case of Au on SiO<sub>2</sub>, it was seen that the Au film piled up around the indenter as the displacement increased.

## References

1. Doerner, M.F. and W.D. Nix, *A method for interpreting the data from depth-sensing indentation*. Journal of Materials Research, 1986. **1**(4): p. 601-609.
2. King, R.B., *Elastic analysis of some punch problems for a layered medium*. International Journal of Solids and Structures, 1987. **23**(12): p. 1657-1664.
3. Pharr, G.M., J.H. Strader, and W.C. Oliver, *Critical issues in making small-depth mechanical property measurements by nanoindentation with continuous stiffness measurement*. Journal of Materials Research, 2009. **24**(03): p. 653-666.
4. Saha, R. and W.D. Nix, *Effects of the substrate on the determination of thin film mechanical properties by nanoindentation*. Acta Materialia, 2002. **50**(1): p. 23-38.
5. Zhou, B. and B.C. Prorok, *A Discontinuous Elastic Interface Transfer Model of Thin Film Nanoindentation*. Experimental Mechanics, 2009. **50**(6): p. 793-801.
6. Zhou, B. and B.C. Prorok, *A new paradigm in thin film indentation*. Journal of Materials Research, 2010. **25**(09): p. 1671-1678.
7. Prorok, B.C., et al., *Micro- and Nanomechanics*. Encyclopedia of Nanoscience and Nanotechnology, 2004. **5**: p. 555-600.
8. Li, X. and B. Bhushan, *A review of nanoindentation continuous stiffness measurement technique and its applications*. Materials Characterization, 2002. **48**(1): p. 11-36.
9. Zhou, B., *Exploration of the Origin of Substrate Effects and Elastic Strain Properties during Thin Film Nanoindentation*, in *Materials Engineering*, 2009, Auburn University: Auburn. p. 144.

10. McElhaney, K.W., J.J. Vlassak, and W.D. Nix, *Determination of indenter tip geometry and indentation contact area for depth-sensing indentation experiments*. Journal of Materials Research, 1998. **13**(5): p. 7.
11. Oliver, W.C. and G.M. Pharr, *An improved technique for determining hardness and elastic modulus using load and displacement sensing indentation experiments*. Journal of Materials Research, 1992. **7**(6): p. 1564-1583.
12. Rar, A., H. Song, and G.M. Pharr, *Assessment of new relation for the elastic compliance of a film-substrate system*. Thin Films: Stresses and Mechanical Properties IX, 2002. **695**: p. 431.
13. Hertzberg, R.W., *Deformation and Fracture Mechanics of Engineering Materials*. 4th ed1996: John Wiley & Sns, Inc.
14. Kulkarni, A.V. and B. Bhushan, *Nano/picoindentation measurements on single-crystal aluminum using modified atomic force microscopy*. Materials Letters, 1996. **29**(4-6): p. 221-227.
15. Branger, V., et al., *Study of the mechanical and microstructural state of platinum thin films*. Thin Solid Films, 1996. **275**(1-2): p. 22-24.
16. Fang, T.-H., W.-J. Chang, and C.-I. Weng, *Nanoindentation and nanomachining characteristics of gold and platinum thin films*. Materials Science and Engineering: A, 2006. **430**(1-2): p. 332-340.
17. Quiñones, C., W. Vallejo, and F. Mesa, *Physical and electrochemical study of platinum thin films deposited by sputtering and electrochemical methods*. Applied Surface Science, 2011. **257**(17): p. 7545-7550.

18. Espinosa, H.D., B.C. Prorok, and M. Fischer, *A methodology for determining mechanical properties of freestanding thin films and MEMS materials*. Journal of Mechanics and Physics of Solids, 2003. **51**: p. 46-67.
19. Furukawa, M., et al., *Surface morphologies of sputter-deposited aluminum films studied using a high-resolution phase-measuring laser interferometric microscope*. Appl. Opt., 1996. **35**(4): p. 701-707.
20. Herman, D.S., M.A. Schuster, and R.M. Gerber, *Hillock Growth on Vacuum Deposited Aluminum Films*. Journal of Vacuum Science and Technology, 1972. **9**(1): p. 515-519.
21. Voutsas, A.T., et al., *Structure engineering for hillock-free pure aluminum sputter deposition for gate and source line fabrication in active-matrix liquid crystal displays*. Journal of Vacuum Science & Technology A: Vacuum, Surfaces, and Films, 1998. **16**(4): p. 2668-2677.